Received: 26 September 2024 | Revised: 17 October 2024 | Accepted: 28 October 2024

DOI: 10.1002/inf2.12653

REVIEW ARTICLE

WILEY

Advanced carbon as emerging energy materials in lithium batteries: A theoretical perspective

Legeng Yu | Xiang Chen | Nan Yao | Yu-Chen Gao | Yu-Hang Yuan | Yan-Bin Gao | Cheng Tang | Qiang Zhang

Tsinghua Center for Green Chemical Engineering Electrification (CCEE), Beijing Key Laboratory of Green Chemical Reaction Engineering and Technology, Department of Chemical Engineering, Tsinghua University, Beijing, the People's Republic of China

Correspondence
Xiang Chen and Qiang Zhang, Tsinghua Center for Green Chemical Engineering Electrification (CCEE), Beijing Key Laboratory of Green Chemical Reaction Engineering and Technology, Department of Chemical Engineering, Tsinghua University, Beijing 100084, the People's Republic of China.
Email: xiangchen@tsinghua.edu.cn and zhang-qiang@mails.tsinghua.edu.cn

Funding information
Beijing Natural Science Foundation, Grant/Award Number: L233004; National Key Research and Development Program, Grant/Award Number: 2021YFB2500300; National Natural Science Foundation of China, Grant/Award Numbers: T2322015, 22109086, 52394170, 52394171, 22109011, 22393900, 22108151; Tsinghua-Jiangyin Innovation Special Fund, Grant/Award Number: 2022JYTH0101; Tsinghua University Initiative Scientific Research Program

Abstract

Lithium batteries are becoming increasingly vital thanks to electric vehicles and large-scale energy storage. Carbon materials have been applied in battery cathode, anode, electrolyte, and separator to enhance the electrochemical performance of rechargeable lithium batteries. Their functions cover lithium storage, electrochemical catalysis, electrode protection, charge conduction, and so on. To rationally implement carbon materials, their properties and interactions with other battery materials have been probed by theoretical models, namely density functional theory and molecular dynamics. This review summarizes the use of theoretical models to guide the employment of carbon materials in advanced lithium batteries, providing critical information difficult or impossible to obtain from experiments, including lithiophilicity, energy barriers, coordination structures, and species distribution at interfaces. Carbon materials under discussion include zero-dimensional fullerenes and capsules, one-dimensional nanotubes and nanoribbons, two-dimensional graphene, and three-dimensional graphite and amorphous carbon, as well as their derivatives. Their electronic conductivities are explored, followed by applications in cathode and anode performance. While the role of theoretical models is emphasized, experimental data are also touched upon to clarify background information and show the effectiveness of strategies. Evidently, carbon materials prove promising in achieving superior energy density, rate performance, and cycle life, especially when informed by theoretical endeavors.

KEYWORDS

carbon energy materials, density functional theory, electrode materials, lithium batteries, molecular dynamics

1 | INTRODUCTION

Due to the growing demand for electric vehicles (EVs), large-scale energy storage systems, and portable electronics, lithium (Li) batteries play an increasingly vital role in modern societies.[1–3] On the one hand, thanks to their efficient "rocking chair" mechanism, Li-ion batteries (LIBs) have become the dominant energy storage

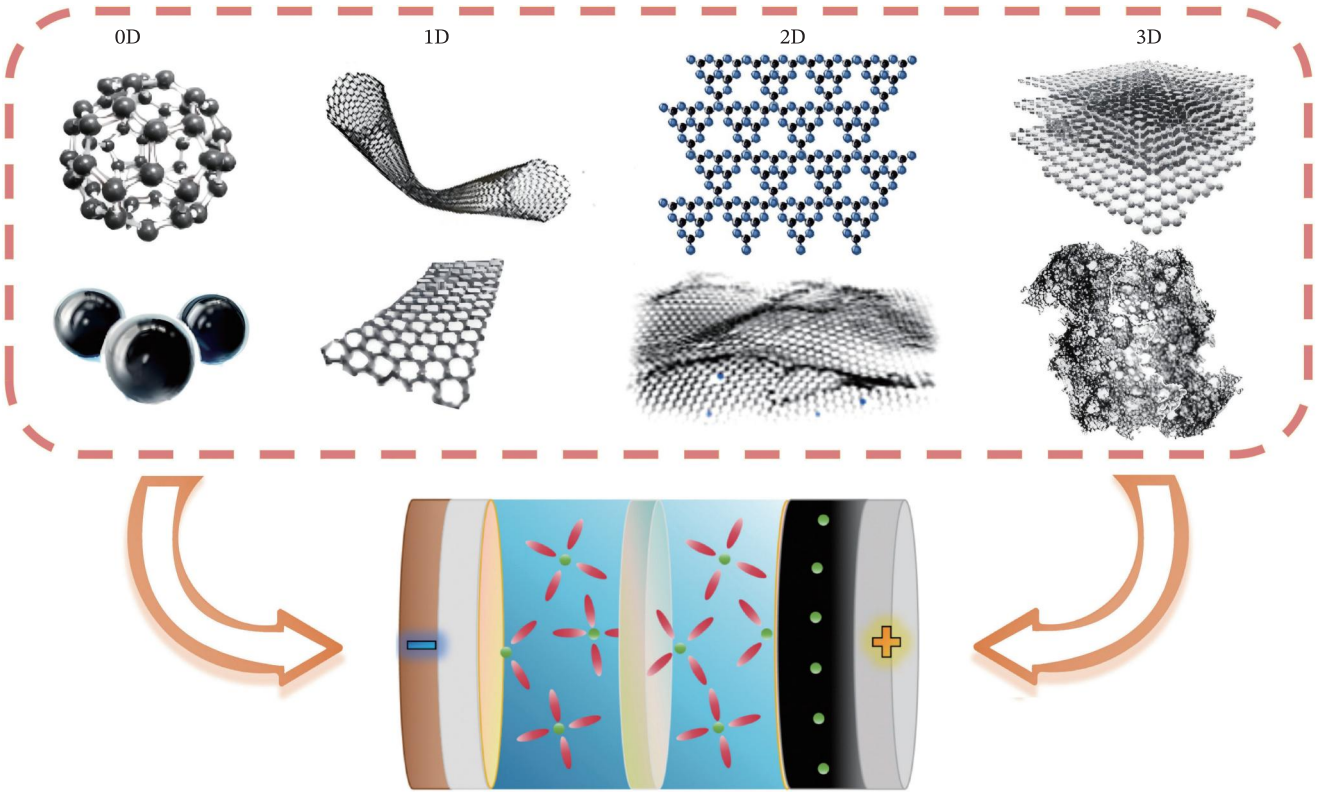

FIGURE 1 Application of carbon materials in Li batteries. From left to right, first column: 0D fullerene (upper) and carbon capsules (lower). Second column: 1D CNT (upper) and GNR (lower). Third column: 2D graphitic carbon nitride (g-C_3N_4, upper) and doped/defective graphene (lower). Fourth column: 3D graphite crystal (upper) and non-crystalline carbon (lower).

solution for commercial EVs and electronic products due to their relatively high energy density and cyclability.[4–12] Nevertheless, new materials and strategies are being actively developed to improve the rate performance and temperature tolerance of LIBs.[13–16] On the other hand, Li metal batteries (LMBs), including Li–S, Li–air, and all-solid-state LMBs, are being revived and improved to unlock higher theoretical capacities by accommodating more active material in the anode (3860 mAh g^{-1} for Li metal anode compared to only 372 mAh g^{-1} for graphite anode).[17–28]

To optimize the energy density, rate performance, and cycle life of Li batteries, carbon materials have become a significant part in the rational design of rechargeable Li batteries. Some applications of carbon materials are fundamental, such as storing Li^+ by allowing intercalation in LIB anode[29] and hosting Li metal deposition in LMBs,[30,31] as well as conducting electrons in sulfur (S) cathode.[32] Some applications are auxiliary, such as electrolyte additives,[33] protective barriers for electrodes,[34] and separator coating.[35]

During the development of these strategies involving carbon materials, theoretical studies employing density functional theory (DFT) and molecular dynamics (MD) play a crucial role in rationally identifying suitable materials and elucidating their working mechanisms. As a quantum mechanical model capable of revealing electron distribution in multiatomic systems by solving the Kohn–Sham equations, DFT has been widely used to determine the stability of materials[36–39] and affinity between species,[40,41] as well as energy change in reaction pathways.[42] Physical movements of atoms and molecules can be further modeled by time-integrating Newton's second law in MD simulations, including ab initio molecular dynamics (AIMD) and classical MD,[43,44] in order to determine equilibrium properties[45–47] or transition processes of atomic systems.[48–50] Although these theoretical models have been widely developed and applied in materials science,[51–59] a comprehensive review from the perspective of theoretical studies on the application of carbon materials in Li batteries is lacking.

In this contribution, we summarize the use of DFT and MD in determining the properties of carbon materials in Li battery technology as well as their interaction with electrode materials and electrolytes. Relevant carbon materials include zero-dimensional (0D) fullerenes and carbon capsules, one-dimensional (1D) carbon nanotubes (CNTs) and graphene nanoribbons (GNRs),

two-dimensional (2D) graphene and its derivatives, and three-dimensional (3D) graphite and non-crystalline carbons (Figure 1). Non-crystalline carbon materials, such as soft carbon and hard carbon, are included. Soft carbon consists of slightly loose carbon sheets graphitizable by heat treatment over 2000°C.[60] Hard carbon, not graphitizable even at 3000°C, consists of highly disordered and curved carbon walls forming large pores, which is typically suitable for sodium (Na) storage.[60,61] First, the electronic structures and conductivity of carbon materials will be explored in Section 2, which is fundamental for understanding their functions in Li batteries. Second, the application of carbon materials in cathode and anode will be discussed in Sections 3 and 4, respectively, with an emphasis on theoretical modeling at an atomic scale. Facts and insights obtained from experimental results are also peripherally touched upon to illustrate background information and practical performances. Lastly, the conclusion section summarizes the applications of carbon materials in Li batteries and the role of DFT and MD in the discovery and development of these materials.

2 | ELECTRONIC STRUCTURES OF CARBON MATERIALS

The small size of carbon atom (C atom) and its unique electronic configuration, $1s^2 2s^2 2p^2$, allow the element to form various allotropes, each of which possesses unique electronic conductivities. Generally, carbon materials conduct electrons because when C atoms are sp^2 hybridized the π electrons are delocalized and can move across the C atom plane. However, the mobility of these π electrons is determined by the different atomic arrangements in carbon materials. This section will explore the electronic conductivities of various carbon materials.

2.1 | 0D carbon materials

0D fullerenes, represented by the famous buckminsterfullerene C_{60}, can be regarded as molecular semiconductors thanks to their entirely sp^2 hybridized C atoms.[62] However, the electronic conductivity of fullerences can be regulated significantly under various circumstances. The bandgap of C_{60} was estimated to be 1.6–1.7 eV according to DFT calculations.[63] Even though some fullerenes theoretically possess near-zero bandgaps (e.g., C_{74} with a bandgap of 0.05 eV), they are kinetically unstable and polymerize readily.[63] However, C_{60} and C_{70} can be modulated into conductors by doping with alkali metals, which partially fill the energy bands from the π orbitals, achieving electronic conductivities of 2–500 S cm^{-1}.[64,65] Superconductivity in modified fullerenes has also been reported,[66,67] but it is still out of the temperature range for practical application in various batteries. For instance, C_{60} doped with cesium (Cs) and rubidium (Rb) renders a transition temperature of only 33 K, which is already among the highest transition temperatures in similar systems.[67,68]

While these fullerenes can be regarded as 0D carbon materials at the nanoscale, carbon capsules can be regarded as 0D materials at a macroscale of hundreds of nanometers. They typically consist of walls of mainly disordered graphene/graphite layers, which are capable of conducting electrons especially when doped with nitrogen (N) and nickel (Ni).[69–71] The electronic conductivity of graphite and amorphous carbon will be discussed in more detail in Section 2.4.

2.2 | 1D carbon materials

GNRs are 1D carbon materials characterized by one-atom-thick narrow strips of graphene.[72–74] Based on the angle θ between the GNR long axis and the zigzag crystallographic direction of the graphene lattice, GNRs can be classified into zigzag graphene nanoribbons (ZGNRs) for $\theta = 0°$, chiral GNRs for $0° < \theta < 30°$, and armchair graphene nanoribbons (AGNRs) for $\theta = 30°$.[75] Due to the quantum confinement effect, most GNRs possess a width-dependent non-zero bandgap,[76–78] in contrast to bulk graphene. As the GNR width increases, the bandgap decreases and eventually approaches 0, which is the bandgap of 2D graphene (Figure 2A).[79] Consequently, wide (130–250 nm) and nearly defect-free GNRs have been experimentally demonstrated to exhibit good electronic conductivities of ~700–950 S cm^{-1}.[80] On top of this general trend, the bandgap is also affected by the remainder of the number of rows divided by 3, where a remainder of 1 exhibits the largest bandgaps for AGNRs.[75] The type of edge of the GNR also has a significant impact on its bandgap, as ZGNRs possess a bandgap between that of $3p + 2$ and $3p + 1$ family AGNRs (Figure 2A).[75]

Despite having a non-zero bandgap, ZGNRs can theoretically be made half-metallic under a transverse electric field.[81] This phenomenon is based on the fact that the charge densities of the two spin states are different at the two edges of a ZGNR, which is revealed by spin-resolved DFT calculations.[81] Under a transverse electric field, the energy levels at the two edges are shifted in opposite directions.[81] As a result, states of only one spin orientation will lie at the Fermi energy level (E_F), which enables the conduction of a spin-polarized electrical current.[81] Another intriguing advantage of electron

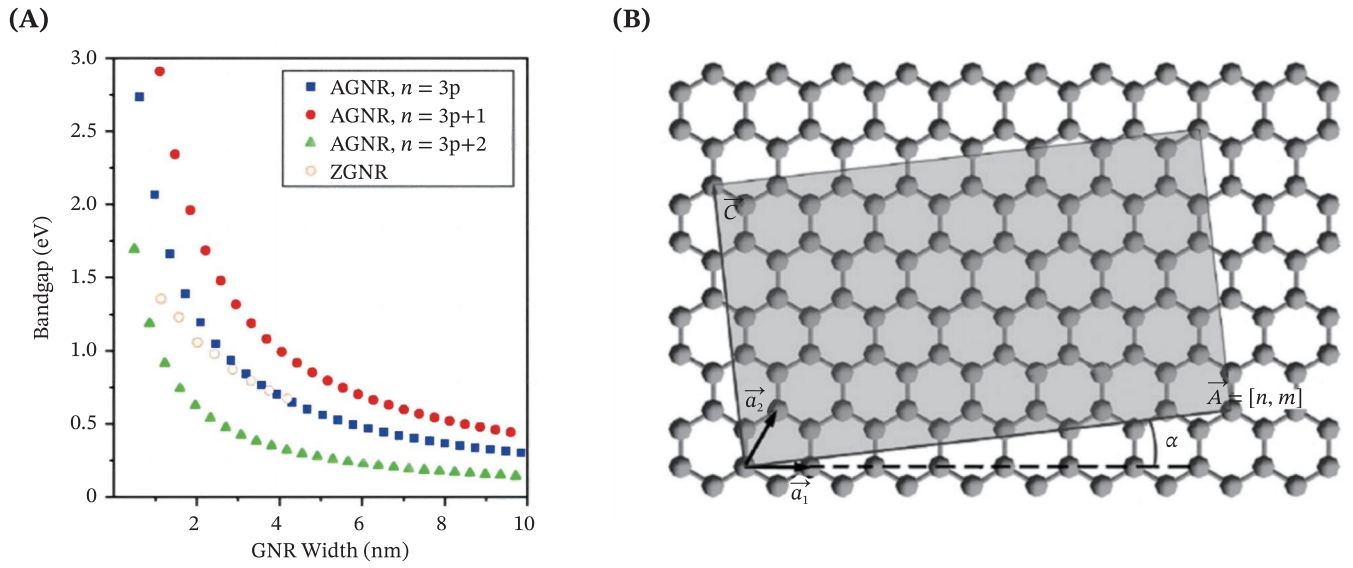

FIGURE 2 Bandgaps in GNRs and chirality of CNTs. (A) Bandgap in AGNRs and ZGNRs with respect to width. The number of rows of C atoms along the width is denoted by n, and p is an integer. As the width of GNR increases, the bandgap approaches 0, which is the bandgap of graphene. Reprinted with permission.[75] Copyright 2021, American Chemical Society. (B) Illustration of CNT chirality before rolling up. $\boldsymbol{a_1}$ and $\boldsymbol{a_2}$ are basis vectors of the graphene plane. $\boldsymbol{A}$, (1, 7) in this example, represents the perimeter of the CNT after rolling up. $\boldsymbol{c}$ represents the direction of the CNT axis. α is the helical angle. Reprinted with permission.[84] Copyright 2007, the Owner Societies.

conduction in GNRs is the possibility of ballistic transport, where electrons are transported without scattering or conductive heating.[82] Such efficient transport has been realized in epitaxial GNRs on a length scale greater than 10 μm.[83]

CNTs consist of rolled-up sheets of single-layer C atoms (graphene) in the sp^2 hybridized state. The orientation and width of the graphene strip to be rolled up are described by the chiral indices, a vector representing the base of the graphene strip taken out from an infinite graphene sheet (Figure 2B).[84] Zigzag CNTs have chiral indices in the form of (m,0), while the chiral indices for armchair CNTs have the form (m,m).[84,85] Due to the variety of diameters and helicity of C atoms, accurately measuring the electronic conductivity of individual CNTs can be challenging, and the results will vary to a large extent based on the geometry.[86] Depending on the diameter and geometric chiral angle, CNTs can appear to be metallic or semiconducting.[85] Zigzag CNTs with a chiral index m that is a multiple of 3 are metallic, and their electronic conductivity decreases with increasing diameter, approaching an asymptotic value of the conductivity of graphene.[85] Other zigzag CNTs are semiconducting, exhibiting a trend of increasing conductivity with diameter, approaching the same asymptote.[85] In contrast, armchair CNTs are conductors at any m, and the conductivity decreases with increasing diameter, approaching the same asymptote.[85]

It is worth noting that similar to GNRs, single-walled CNTs can also theoretically exhibit ballistic electron transport, where electrons propagate efficiently along the axis of the tube without scattering or conductive heating.[87,88] The excellent electronic conductivity of single-walled CNTs make them ideal candidates for electrode conductive fillers.[89–91] Moreover, according to DFT calculations, N-doping can further enhance the electronic conductivity of semiconducting CNTs by closing or shortening the bandgap.[92]

2.3 | 2D carbon materials

Graphene is a 2D carbon allotrope consisting of only one layer of sp^2 hybridized C. It exhibits a unique band structure known as the Dirac cone, which simultaneously resembles a semiconductor with zero density of states and a metal with no gap between the valence and conduction band.[93] Thanks to the zero bandgap, graphene affords an extraordinary electronic conductivity of up to 10^6 S cm^{-1}.[94] Ballistic transport of electrons in graphene has also been observed experimentally, where electrons can propagate without scattering over micrometers of lengths.[93] While the in-plane conductivity of graphene is isotropic[85] and high, it is relatively difficult for electrons to be transported from one graphene flake to another. When fabricated into macroscopic conductor materials,

graphene displays a reduced conductivity depending on the in-plane conductivity, out-of-plane connections, packing density, and flake size.[94] To enhance the conductivity of graphene, doping can be introduced. For instance, pyrrolic N can improve the electronic conductivity by providing delocalized electrons while maintaining the sp^2 hybridized graphitic structure.[95] With proper defect-engineering and doping strategies, macroscopic graphene-based nanomaterials can render an electronic conductivity on the same order of magnitude as that of copper (Cu) and silver (Ag).[94]

In contrast to graphene, the 2D compound material g-C_3N_4 possesses a poor electronic conductivity with a bandgap of ~2.7 eV.[96] The conductivity of g-C_3N_4 can be improved by several doping strategies.[97] For instance, phosphorus (P)-doping has been reported to improve g-C_3N_4's conductivity by 4 orders of magnitude, achieving a conductivity above 10^{-9} S cm^{-1}.[98] Besides, according to DFT calculations, C self-doping by substituting bridging N atoms (i.e., replacing those N atoms singly bonded to three C atoms with C atoms) can create delocalized big π-bonds and reduce the bandgap of g-C_3N_4, improving its electronic conductivity.[99] Bromine (Br)-doping[100] and C–Fe co-doping[101] have also been reported to narrow the bandgap and improve electronic conductivity.

2.4 | 3D carbon materials

Theoretically, a perfect graphite crystal consists of only graphene layers stacked in a regular ABAB pattern. Given the structural anisotropy, its electrical conductivity also varies with the direction of charge transfer. Similar to graphene, the conduction band slightly overlaps the valence band in graphite,[102] allowing electron transport within the layer plane. However, it is relatively difficult for electrons to be transported from one graphene layer to the next, so the electronic conductivity perpendicular to the layer planes is only about a hundredth of that along the layer planes.[102] The temperature dependence is another intriguing fact about the electronic conductivity of graphite. While metals exhibit reduced electronic conductivity with increasing temperature due to electron scattering, graphite exhibits this trend only at very low temperatures.[102] As the temperature gets higher, its conductivity levels off[102] and eventually rises,[103] since more electrons are excited to the conduction band as charge carriers. Intercalation also determines the electronic conductivity of graphite for two reasons. First, the Fermi surface and electron–phonon coupling can be drastically modified upon intercalation due to the distancing of the graphene layers.[104] Second, these intercalates can interact with the graphene layers by donating or accepting electrons.[104] The conductivity of an intercalated graphite is estimated to reach about three times that of copper at room temperature, based on first-principles calculations within a tight-binding framework.[104]

In less crystalline 3D carbon materials, the electronic conductivity is more complex and depends on microscopic structure and macroscopic morphology. In natural graphite sheets formed by compressing exfoliated natural graphite, the through-plane conductivity ranges from 3 to 25 S cm^{-1} while the in-plane conductivity ranges from 500 to 1700 S cm^{-1}, mainly depending on sheet density.[105] Introducing sp^3 C atoms makes the structure even more amorphous and more rigid. Since the σ–σ* transition poses a huge energy gap (5.5 eV bandgap for diamond), amorphous carbons typically exhibit poorer electronic conductivity (e.g., typically 10^{-9}–10^{-3} S cm^{-1} at room temperature) and less conductivity anisotropy[103] than graphite, depending on the amount and distribution of sp^2 sites.[106] To be transported in an amorphous carbon material, electrons need to either hop between neighboring sp^2 islands embedded in an sp^3 matrix or hop in the band tails.[106]

3 | THE APPLICATION OF CARBON IN LI ION BATTERY CATHODE

3.1 | 0D carbon

Although relatively uncommon, the possibility of applying 0D fullerenes in Li battery cathodes has been investigated from a few aspects. On the one hand, C_{60} has been confirmed to be a valid organic cathode active material by allowing Li^+ intercalation.[107] DFT calculations reveal that each C_{60} molecule can accommodate 3 Li^+ while staying stable, which is consistent with 3 plateaus observed in galvanostatic intermittent titration tests.[107] Initially, 0D fullerenes were thought to be unfit for the cathode material because their reduction products dissolve readily in solvents such as propylene carbonate.[108] However, an ether-based electrolyte solution was later proposed to be compatible with C_{60} cathode, namely Li bis(trifluoromethane)sulfonimide (LiTFSI) in dimethyl ether and dioxolane, exhibiting a capacity of 90 mAh g^{-1} after 50 cycles and a rate performance of 77 mAh g^{-1} at 500 mA g^{-1}.[107] Acetylene black was added as the conductive agent in this cathode, and the aluminum (Al) foil current collector was also coated with conductive carbon.[107]

On the other hand, C_{60} can be used as a supplementary material to enhance the performance of other active cathode materials. Transition metal oxides are popular

active cathode materials due to their excellent energy density, bulk stability, and conductivity,[10] but they suffer from poor interfacial stability in contact with a liquid electrolyte when charged to a high potential (e.g., 4.4 V vs. Li/Li^+), marked by electrolyte decomposition, gas evolution, dissolution of transition metal ions, and solid phase transformation.[33] To protect the cathode from such aging phenomena, malonic acid-decorated C_{60} has been demonstrated as a valid electrolyte additive that suppresses interfacial side reactions by scavenging water molecules and superoxide radicals while forming a protective interfacial layer via polymerization with ethylene carbonate (EC) molecules.[33] Alternatively, the cathode can be directly coated with a thin film of polymerized C_{60} through plasma-assisted thermal evaporation, which prevents side reactions and transition metal dissolution while enhancing interfacial kinetics.[109] Another promising active cathode material is elemental S thanks to its ultrahigh energy density and elemental abundance, but it suffers from the notorious polysulfide shuttle effect, where intermediate polysulfide ions dissolve into the electrolyte and migrate back and forth between the cathode and the anode, leading to self-discharge and capacity fading.[110] To inhibit this shuttle effect, C_{60} can be made into an interlayer of nanorods placed between the separator and the S cathode, which blocks the diffusion passage of Li polysulfides by physical adsorption and chemical bonding and confines them within the cathode region.[111]

Alternatively, S-containing species can be confined in carbon capsules[112] with porous sidewalls, inside which soluble Li polysulfides may be trapped and converted into insoluble polysulfides.[71] Such carbon capsules can be doped with S and N to enhance the chemisorption of Li polysulfides.[71] Besides, they also help the electron transport to the elemental S inside, providing an electronic conductivity of 47 S cm^{-1}.[71] Additionally, single-atom $Ni–N_5$ catalytic sites have been further introduced into carbon capsules, which can accelerate the otherwise sluggish Li polysulfide redox conversion kinetics.[70]

3.2 | 1D carbon materials

1D carbon materials, namely GNRs and CNTs, have the potential to work with active cathode materials that would perform poorly if used alone. For example, V_2O_5 is a potential cathode material with an outstanding capacity of 294–440 mAh g^{-1}, which is much higher than that of routine cathodes like $LiCoO_2$ (theoretically 274 mAh g^{-1} and practically 165 mAh g^{-1} at a charge cut-off voltage of 4.35 V[10]) and $LiFePO_4$ (170 mAh g^{-1}).[113] However, it suffers from degradation upon Li^+ diffusion and poor electronic conductivity.[113] By loading 40 wt% nanocrystalline V_2O_5 in a framework of GNRs, the cathode can be stabilized and made conductive, achieving a high capacity of 278 mAh g^{-1} at 0.1 C.[113] Moreover, N-doped GNRs can be combined with S cathode to inhibit the shuttle effect by trapping soluble Li polysulfide intermediates around the N doping sites.[114] The binding effect of different types of N-doped GNRs with Li polysulfides has been systematically investigated using DFT (Figure 3).[114] Pyrrolic N is shown to provide an extra binding energy of 1.12–1.41 eV, while pyridinic N provides an extra binding energy of 0.55–1.07 eV.[114]

Since N is not the only element that can afford strong binding with Li sulfides, the effect of other doping elements has been systematically investigated in a similar setting with DFT. Figure 4A exhibits a variety of dopant elements, including boron (B), N, oxygen (O), fluorine (F), P, S, and chlorine (Cl), under possible chemical environments in a GNR.[115] As revealed by binding energy calculations, N or O dopant significantly enhances the binding between the GNR and Li sulfides through dipole–dipole electrostatic interaction (Figure 4B).[115] By contrast, B, F, S, P, and Cl monodopants result in a weakened binding.[115] A volcano plot (Figure 4C) can be achieved by mapping the binding energies against the electronegativities of the dopant elements in the second period, where the binding strength reaches a peak with N and O but drops with F.[115] Despite the strong electronegativity of F and thus its electron-withdrawing capability from C through the σ-bond, its filled p orbitals release some of the negative charge back to C, resulting in a weakened electrostatic attraction with Li sulfides.[115]

Beyond mere binding with Li sulfides, the function of heteroatom-doped GNRs extends to electrochemically catalyzing the polysulfide reduction reactions. Polysulfide conversion from soluble Li_2S_4 to solid Li_2S accounts for 75% of the total discharge capacity but suffers from sluggish kinetics.[42] To elucidate the mechanisms of this complex conversion involving 6 electron transfers and design electrocatalysts correspondingly, DFT models have been systematically established for the calculation of Gibbs free energies in the intermediate steps.[42] Six reaction pathways are proposed (Figure 5A): two pathways are symmetric, involving the formation of Li_2S_2 from Li_2S_4; four pathways are asymmetric, involving the direct formation of a quarter of the final product Li_2S from L_2S_4.[42] The Gibbs free energy evolution depends on the reaction pathway and the dopant atom (Figure 5B,C).[42] The adsorption Gibbs free energy of Li polysulfide radicals largely determines the reaction overpotential and rate-determining step.[42] This understanding of polysulfide electrochemical conversion on GNRs guides the choice of appropriate heteroatoms for efficient electrocatalysts,

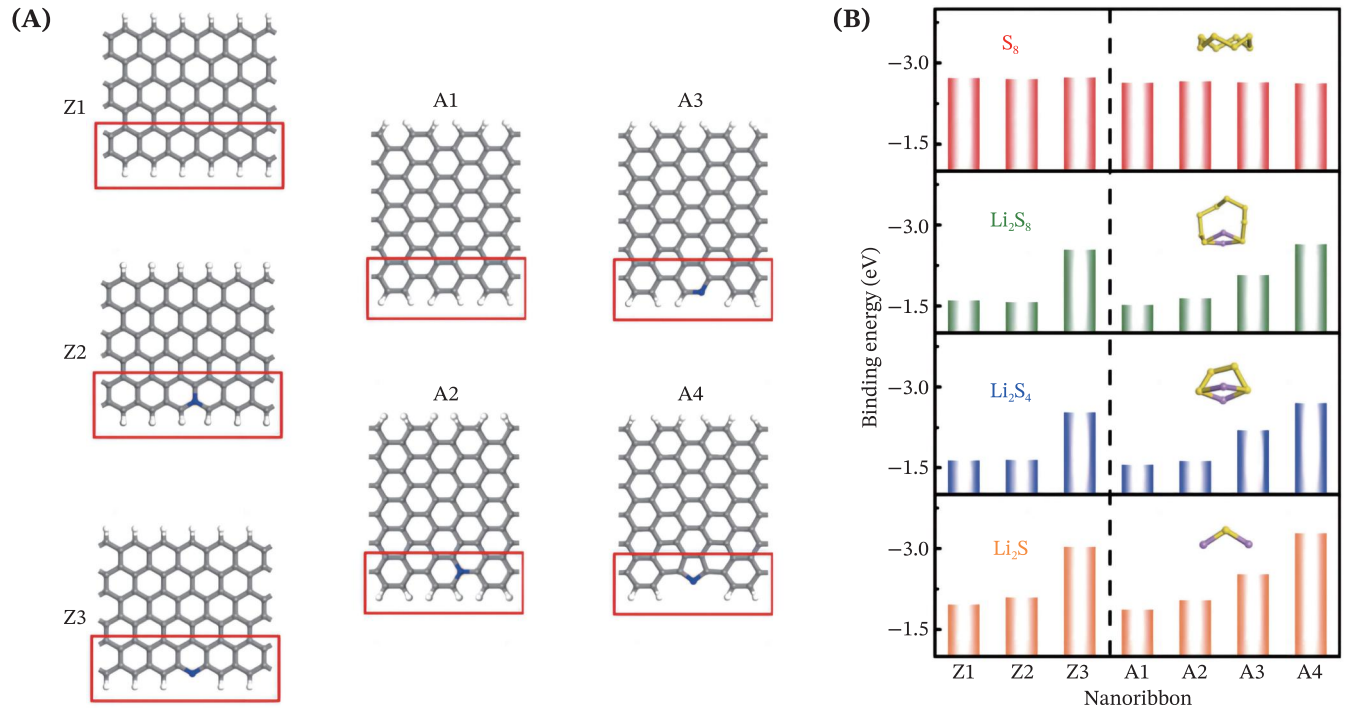

FIGURE 3 Binding effect of N dopant atoms in GNRs with Li sulfides. (A) Atomic configuration of pristine zigzag GNR (Z1), zigzag GNR with quaternary N (Z2), zigzag GNR with pyridinic N (Z3), pristine armchair GNR (A1), armchair GNR with quaternary N (A2), armchair GNR with pyridinic N (A3), and armchair GNR with pyrrolic N (A4). (B) Corresponding binding energies of the GNRs with S_8, Li_2S_8, Li_2S_4, and Li_2S. Reprinted with permission.[114] Copyright 2015, IOP Publishing.

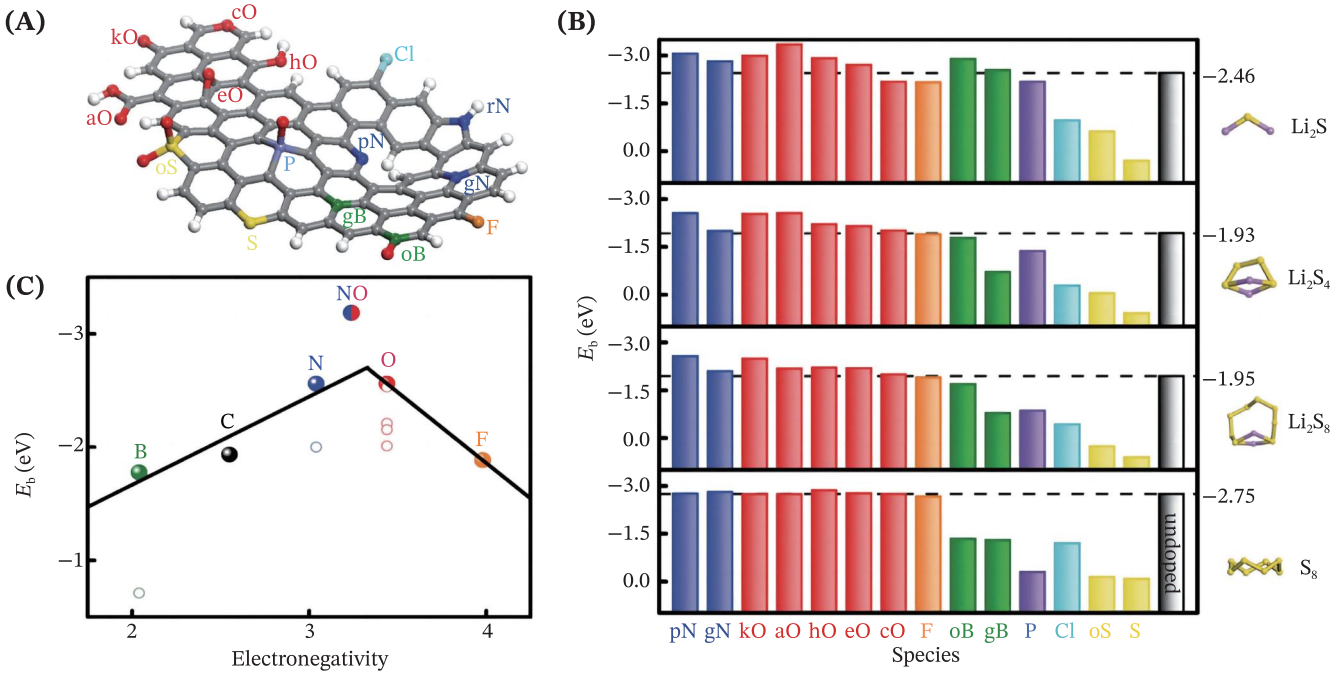

FIGURE 4 Binding effect of various dopant heteroatoms in GNRs with Li sulfides. (A) Nomenclature of the investigated heteroatoms within GNRs. Lower-case letter before element symbol denotes the chemical environment of the dopant atom. (B) Corresponding binding energies of the heteroatom-doped GNRs with Li_2S, Li_2S_4, Li_2S_8, and S_8. (C) Binding energy with Li_2S_4 versus the electronegativity of the dopant element (C for undoped GNR). The circle labeled as "NO" represents (N, O)-co-doped GNR. The strongest binding energy achievable for each element is marked with solid circles, and the hollow circles represent weaker forms of binding for each corresponding element. Reprinted with permission.[115] Copyright 2016, Wiley-VCH.

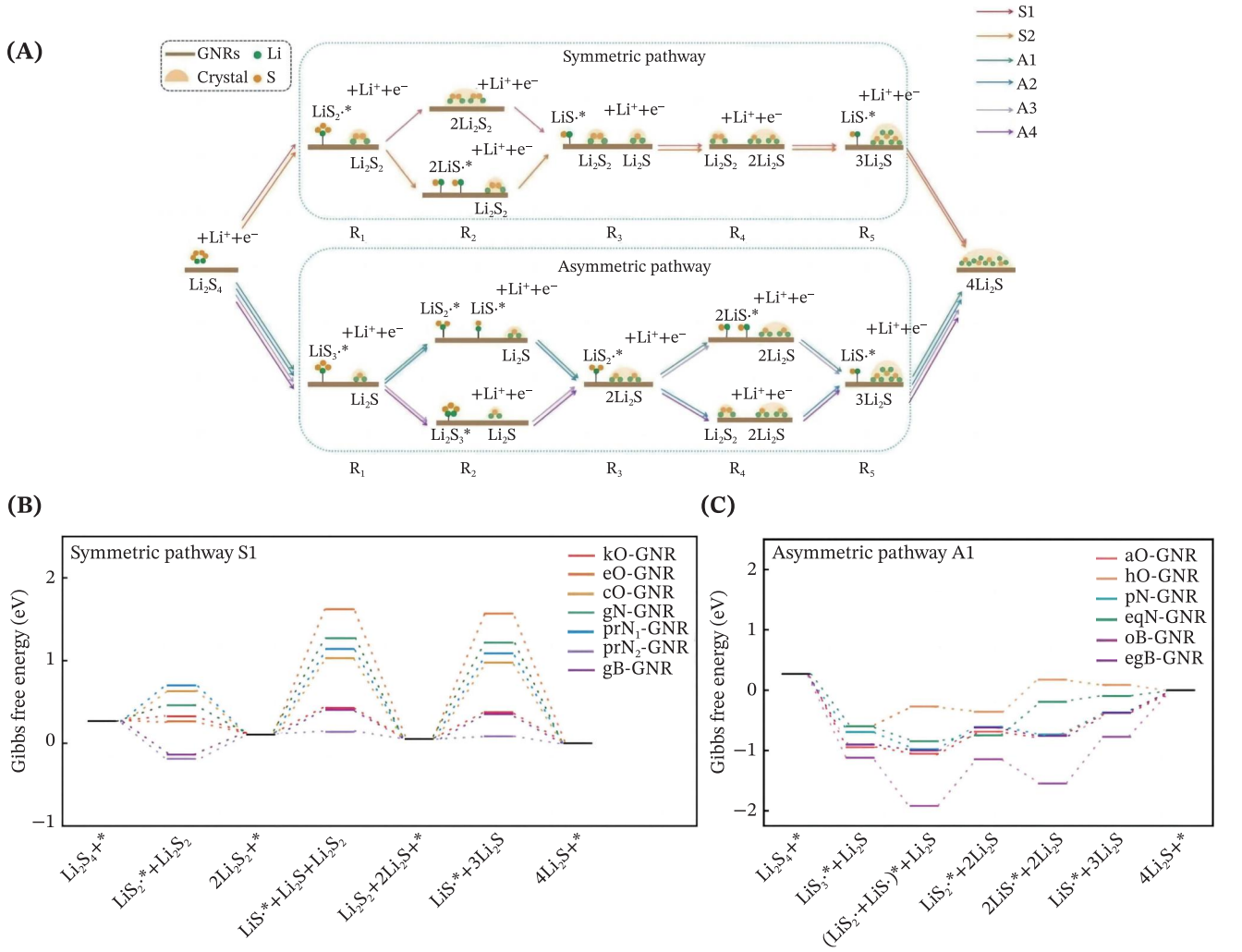

FIGURE 5 Electrocatalysis model of heteroatom-doped GNRs for polysulfide conversion from Li_2S_4 to Li_2S. (A) Six possible reaction pathways, including two symmetric pathways (S1 and S2) and four asymmetric pathways (A1, A2, A3, and A4). Gibbs free energy evolution at 2.15 V vs. Li/Li^+ along pathway (B) S1 or (C) A1 at different doped GNRs. Reprinted with permission.[42] Copyright 2022, Wiley-VCH.

which accelerate the reaction kinetics and ultimately enhance the rate performance while avoiding the shuttle of polysulfides.[42]

Similar to working with GNRs, S cathode can also be made into a composite electrode by combining with doped CNTs[116] or g-C_3N_4 nanotubes, a structure analogous to CNTs but with ultrahigh N content.[117] Its high specific surface area (143 $m^2\ g^{-1}$) with abundant pores allows for a high S loading rate of 74.7 wt%.[117] Apart from alleviating volume change during cycling and improving electronic conductivity just like the commonly used CNTs,[118–120] g-C_3N_4 nanotubes can especially suppress the Li polysulfide shuttle effect by adsorbing the polysulfide species onto the N active sites.[117] This strategy is comparable to the use of GNRs and carbon capsules discussed in Section 3.1.

3.3 | 2D carbon

Graphene can be applied as a non-encapsulating host structure for the S cathode in Li–S batteries, where Li_2S can grow either in a 3D mode or a bilayer mode as revealed by AIMD.[121] The deposition of Li_2S on graphene can be made more controllable by introducing surface defects, including pyridinic N and single vacancy.[122] According to DFT and AIMD simulations, these defects promote the nucleation of Li_2S clusters on these sites and make them grow in a spherical pattern instead of a lamellar pattern as with pristine graphene.[122] The defects also bind Li_2S tightly and serve as pathways for electron transfer between the active material and graphene substrate, which is essential for preventing the occurrence of "dead S" and maintaining an electrochemically active interface.[122,123]

More generally, graphene can also be used as a conductive additive in other cathode systems, such as $LiCoO_2$, where its performance depends on the graphene's surface chemistry and sheet size.[124] The graphene-based conductive agents have been strongly considered in cathode for rechargeable batteries.

3.4 | 3D carbon

Given the structural diversity of carbon materials, S hosts can certainly be converted into complex 3D shapes to allow room for nuanced design strategies, potentially combining the advantages of low-dimensional materials.[125–130] For instance, a 3D hierarchical structure of porous reduced graphene oxide has been engineered to serve as the S hosts, where each layer is modified with N-doped nanoarrays.[89,131] An extra compact graphene layer covers the porous stack of layers, in order to physically block the polysulfides from leaving the cathode.[131] The dopant N atoms in the nanoarrays chemically immobilize the polysulfide species.[131] Consequently, the shuttle effect is successfully suppressed, achieving a capacity retention of 99.94% per cycle for 500 cycles.[131]

More generally, 3D carbon structures can also be applied in other cathode systems, such as Li Fe phosphates and silicates, to enhance conductivity and optimize Li storage performance.[132,133]

4 | CARBON MATERIALS IN EMERGING ANODES

4.1 | 0D carbon

The feasibility of 0D fullerene derivatives as active anode has been explored with the aim of surpassing the charge capacity of routine graphite anode (372 mAh g^{-1}) while offering a precise structure at a molecular level.[134] The C_{60} derivatives exhibit charge capacities from high to low of 861 mAh g^{-1} for carboxyl C_{60}, 404 mAh g^{-1} for ester C_{60}, 170 mAh g^{-1} for pristine C_{60}, and 83 mAh g^{-1} for piperazine C_{60}.[134] The superior capacity of carboxyl C_{60} is attributed to strong Li^+ binding sites provided by the carboxyl group, electron donation to C_{60} cage, large lattice void space, and high specific area due to carboxyl functionalization.[134] Hydrogenated fullerenes ($C_{60}H_x$) have also been tested to maximize Li storage capacity.[135] Each $C_{60}H_x$ molecule can store ~16 Li^+, delivering a capacity of 588 mAh g^{-1} at ~0.1 C for over 600 cycles.[135] Among various H contents, $C_{60}H_{18}$ exhibits the optimal lithiation capacity.[135] DFT calculations reveal that Li atoms tend to adsorb around 3 specific C sites in $C_{60}H_{18}$ rather than being uniformly distributed over the C cage.[135] The hydrogenation breaks the π-bonds and induces negative charge sites on the cage surface, contributing to the stronger binding with Li^+ than pristine C_{60} and hence its superior capacity.[135] Interestingly, Li adsorption causes an expansion of this anode and leads to its pulverization, but it is regarded as a helpful routine for electrode activation by exposing more active surfaces, resulting in an increasing capacity over the first 250 cycles.[135]

Besides serving as active anode materials, 0D fullerenes can also be applied as a supplementary strategy to help Li metal anodes avoid dendrite growth. By introducing a bilayer interphase of dense C_{60} and magnesium (Mg) metal on top of Li foil via vacuum evaporation deposition, Li dendrites can be effectively suppressed, exhibiting a long cycle life over 200.[136] At the same time, this strategy also protects the Li metal anode from humidity.[136] A similar strategy involves constructing a silver@fullerene interphase bilayer placed on a Cu foam current collector.[137] Based on DFT calculations of binding energies with Li^+, Ag is lithiophilic (−1.86 eV) while C_{60} is lithiophobic (−0.69 eV) with a high nucleation barrier.[137] The lithiophilic Ag layer pulls Li^+ into guided uniform deposition—a phenomenon typically observed in many Ag–C or comparable systems[138–143]—while the lithiophobic C_{60} layer regulates a uniform Li^+ flux, resulting in a sandwiched Li plating between the two layers with minimal dendrite growth.[137] Alternatively, nitro-C_{60} at 5 mM concentration can be utilized as an electrolyte additive to suppress Li dendrite growth.[144] At the anode–electrolyte interface, nitro-C_{60} molecules gather at electrode protuberances due to electrostatic interactions and then get reduced into C_{60} and NO_2^-.[144] C_{60} precipitates from the electrolyte and fills the grooves between Li protuberances, thereby smoothing out the anode surface and suppressing dendrites.[144] At the same time, NO_2^- reacts with metallic Li, producing a compact and stable N-rich solid electrolyte interphase (SEI), which protects the Li anode and allows for fast Li^+ transport.[144]

As for carbon capsules, they have been utilized in protecting the silicon (Si)-based anode, which suffers from drastic volume change during charge and discharge.[69] By encapsulating Si nanoparticle clusters, the carbon capsules create space for the structural breathing of Si, effectively preventing the active material from pulverization.[69] The specific surface area of the composite is kept very low, which leads to stable SEI and therefore superior initial Coulombic efficiency compared to coating each Si nanoparticle with carbon.[69]

4.2 | 1D carbon

GNRs have been explored as the Li-storing material in LIB anode. DFT calculations suggest that ZGNRs present a binding energy with Li^+ that is about 50% stronger than

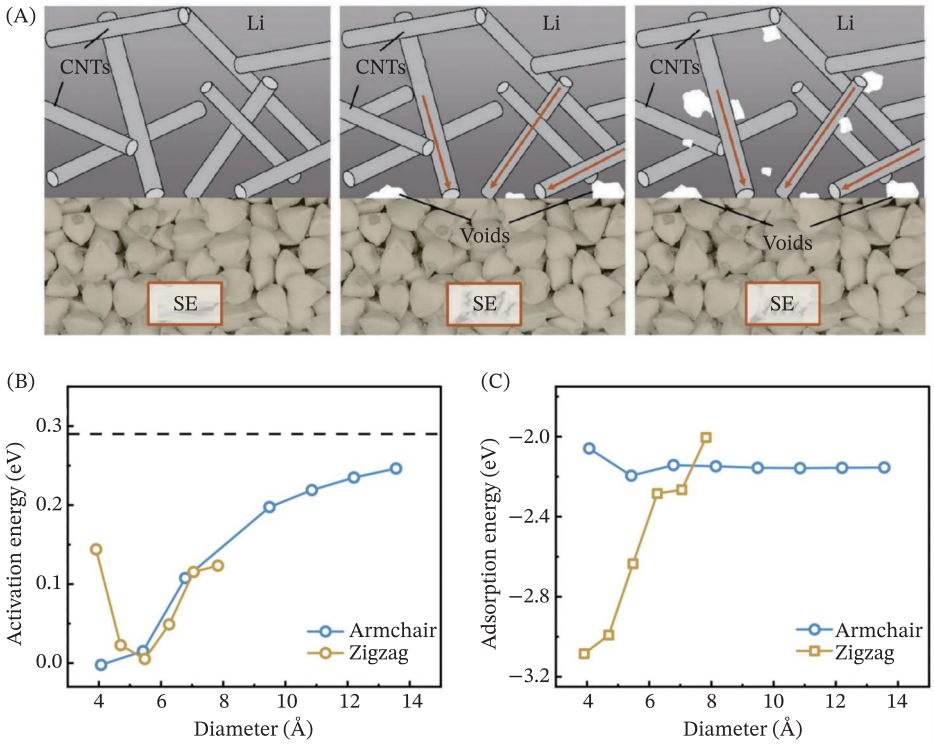

FIGURE 6 CNTs for dendrite suppression via Li^+ transport enhancement. (A) Schematic diagrams showing void formation during fast stripping and the role of CNTs as a contact mediator between Li metal and SE. Reprinted with permission.[149] Copyright 2022, The Authors, Published by Wiley-VCH. (B) Calculated activation energy of Li^+ transport and (C) adsorption energy of Li^+ in CNTs with respect to tube diameter. Reprinted with permission.[151] Copyright 2023, AIP Publishing.

that of graphene, indicating that the edge effect promotes Li^+ storage.[145] The introduction of N dopants further enhances the Li^+ storage capacity by producing topological defects.[146]

GNRs have also been applied as complementary materials in LIB anodes to facilitate electron transport and buffer volume change. For instance, Fe_3O_4 has been employed as an anode with a high theoretical reversible capacity of 928 mAh g^{-1}. However, it suffers from drastic volume change during lithiation and de-lithiation, which induces electrode pulverization.[147] To relieve the strain caused by volume changes, Fe_3O_4 particles can be grown in a scattered manner on GNRs and wrapped with a soft layer of graphene.[147] Apart from providing space to allow volume change, this nanostructured arrangement also facilitates electron and ion transport to the active sites for Li^+ storage.[147] The strategy of distributing active nanoparticles in GNRs also works for SnO_2 anode, achieving a high reversible discharge capacity of 1130 mAh g^{-1} and retains ~825 mAh g^{-1} after 50 cycles at 0.1 A g^{-1}.[148]

A similar strategy has also been devised using CNTs to mitigate the volume change problem for tin (Sn) anode, which is well known for its outstanding volumetric capacity (2111–7316 mA h cm^{-3}, ~3–9 times that of graphite).[20] By encapsulating Sn nanoparticles in robust and conductive frameworks of double-walled graphene tubes, the volume change is buffered while the active material is secured within the tubes, achieving a high volumetric energy density of 1252 W h L^{-1} and reversible capacity retention above 95% after 500 cycles.[20] Similarly, single-walled CNTs have also been demonstrated as an effective conductive network for Si-based anodes by affording superior tensile response and Li^+ diffusivity.[90,91]

CNTs can suppress dendrite growth on working Li metal anode in all-solid-state batteries.[149,150] When Li metal is stripped very quickly during discharge, voids appear at the interfaces between the Li metal and solid electrolyte (SE) (Figure 6A).[149] This pore formation leads to loss of contacts at the interfaces and the tendency of dendrite growth during the subsequent charging process due to surface heterogeneity.[149] When CNTs are incorporated in the body of the Li metal anode, they facilitate Li^+ transport from the bulk of the anode to the SE, resulting in a relatively homogeneous 3D stripping of the anode.[149] From a theoretical point of view, the conductance of Li^+ inside CNTs depends on their chirality and diameter.[151] According to DFT calculation results, the activation energy of Li^+ diffusion increases with tube

diameter (Figure 6B) for armchair CNTs.[151] For zigzag CNTs, the activation energy reaches a minimum (10 meV) with a tube diameter of 5.5 Å, providing an ultralow Li^+ diffusion barrier compared to routine solid electrolyte materials.[151] The origin of the low energy barrier is related to the change in the adsorption energy of Li^+ with respect to tube diameter (Figure 6C).[151] As the tube diameter increases, the adsorption energy does not change significantly for armchair CNTs but becomes significantly less negative for zigzag CNTs, suggesting the weakened interaction with Li^+ in the latter case.[151]

It is worth noting that Li^+ is found to be able to diffuse through the walls of CNTs if the latter has topological defects, such as 10-membered rings.[152] Even a 9-membered ring requires an energy barrier of only 9.69 kcal mol^{-1} to pass through.[152]

Thanks to its light weight and good electronic conductivity, CNTs can serve as current collectors for high-energy-density LIBs, so long as the CNTs are properly passivated to avoid excessive reaction with the electrolyte during cycling.[153] Pouch cells with such CNT current collectors have been reported to offer 50% higher energy density compared to those with conventional metal current collectors.[153]

4.3 | 2D carbon

When used as anode hosts for Li batteries, graphene can achieve a theoretical capacity of 744 mAh g^{-1}[154] or even higher depending on the disorder of the graphene nanosheets.[154,155] It is worth briefly noting herein that graphdiyne, a 2D carbon material comprising sp^2- and sp-hybridized C atoms, can also store Li in a similar manner as graphene, affording an experimental reversible capacity of 520 mAh g^{-1} after 400 cycles at a current density of 500 mA g^{-1}.[156] With the large surface-to-volume ratio of the graphene agglomerate in the shape of flower-petals, abundant Li^+ are bound to both sides of the graphene sheets, as well as the edges and covalent sites.[157] Furthermore, introducing vacancy defects on graphene can further increase the Li/C ratio by affording an extra potential trap for Li^+, as revealed by DFT calculations.[158] Besides, double vacancy and higher-order defects allow Li^+ to diffuse in the direction perpendicular to the graphene sheets by reducing the diffusion barrier from 8.74 to 0.54 eV, thereby enhancing the diffusion energetics of the anode.[158] Doping graphene with N can also render a large number of surface defects, which enhances its reversible discharge capacity to almost double that of pristine graphene tested in experiments.[159] First-principles calculations involving the deposition of multiple Li atoms demonstrate that graphene nanosheets doped with pyridinic N exhibit the highest theoretical Li storage capacity (1262 mAh g^{-1}) among various N-doped graphene nanosheets.[160]

N-doped graphene can regulate the morphology of Li deposits. On the one hand, incorporating graphene flakes in Li metal anode, regardless of doping, is an effective strategy for preventing dendrite growth, because it affords a conductive scaffold with a huge surface area to maintain a very low local current density.[161] On the other hand, when applied as the deposition substrate for metallic Li, the dopant N atoms can serve as preferential deposition sites that guide the location of Li nuclei formation. This strategy encourages Li to deposit specifically at these lithiophilic sites, rather than depositing randomly at first followed by repeated deposition at existing dendritic sites (Figure 7A,B).[162] The dopant N atoms are shown to have a high affinity with Li^+, as suggested by DFT calculations of binding energy.[162] Among various types of N dopant atoms, pyrrolic N exhibits the strongest binding energy of −4.46 eV, compared to only −2.57 eV for copper.[162] In practice, N-doped graphene can be made into an aerogel to serve as the anode host material for Li metal deposition.[163] Thanks to the guided Li deposition, large pore space, and reduced current density, the aerogel anode can achieve a Coulombic efficiency of 99% for over 150 cycles at 0.5 mA cm^{-2} with a fixed capacity of 1.0 mAh cm^{-2}.[163] Apart from N doping, the lithiophilicity of other dopants has also been systematically studied using DFT (Figure 7C).[164] Depending on the doping environment, some dopant elements, namely B, N, O, P, and S may exhibit superior lithiophilicity compared to pristine graphene, while halogen dopants decrease the lithiophilicity.[164] The strongest lithiophilicity is shown by O-doped graphene among single-doped ones and O–B co-doped graphene among double-doped ones.[164] This doping design strategy can also be extended to Na and potassium (K) metal batteries, where O–B, O–S, and O–P co-doping strategies are predicted by DFT calculations to offer the highest sodiophilicity or potassiophilicity.[165]

Since Li plating will be guided toward the lithiophilic sites, these sites should be homogeneously distributed in 3D carbon hosts. This homogeneity can be achieved by constructing a 2D framework through covalently linking porphyrin molecules, which each serve as a lithiophilic unit with 4 electron-rich pyrrolic N atoms (Figure 8A).[166] The porphyrin framework affords a significantly stronger binding with Li than graphene and even N-doped graphene by 0.68 and 0.39 eV, respectively (Figure 8B).[166] The porphyrin framework can be synthesized into a hybrid working electrode by combining with graphene, which prevents the stacking of porphyrin frameworks and increases the overall conductivity.[166] As evidenced by experimental measurements, a much smaller

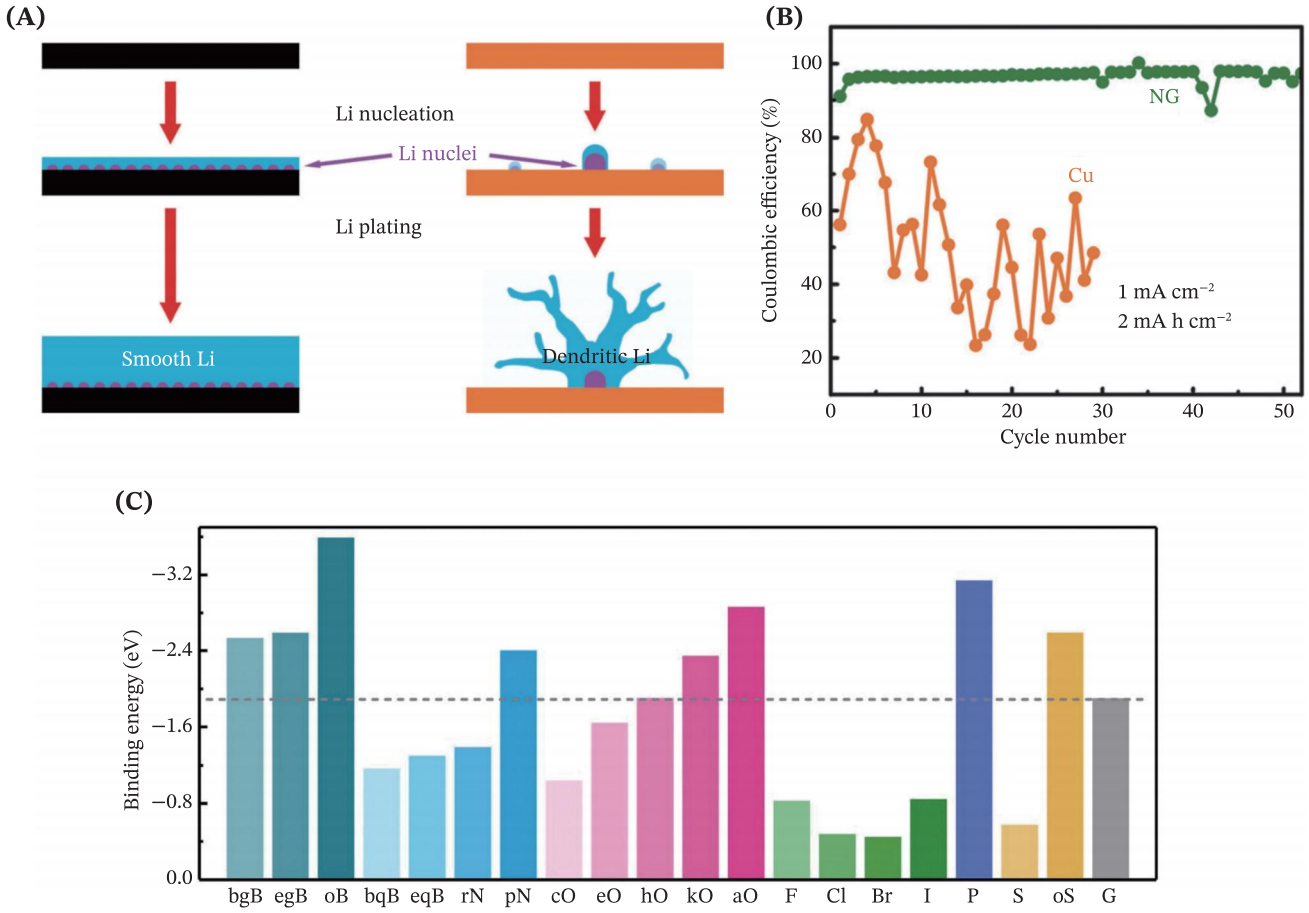

FIGURE 7 Lithiophilic dopant atoms in graphene guides uniform Li metal deposition. (A) Schematic illustration of the effect of N-doped graphene on Li metal deposition morphology. Left: guided Li deposition at lithiophilic dopant sites results in smooth Li metal. Right: unguided Li deposition at copper electrode results in dendrite growth. Reprinted with permission.[162] Copyright 2017, Wiley-VCH. (B) Coulombic efficiency of Cu foil and N-doped graphene (NG) electrode with a cycling capacity of 2.0 mAh cm^{-2} at a current density of 1.0 mA cm^{-2}. Reprinted with permission.[162] Copyright 2017, Wiley-VCH. (C) DFT-calculated binding energy with Li^+ of various dopant atoms in a graphene sheet, compared to pristine graphene (G). Reprinted with permission.[164] Copyright 2019, The Authors, published by the American Association for the Advancement of Science.

nucleation overpotential is needed for the porphyrin framework hybrid electrode (14.6 mV) than a copper electrode, pure graphene electrode, or the N-doped graphene electrode at a consistent current density of 0.5 mA cm^{-2} (Figure 8C).[166] The superior lithiophilicity of the porphyrin framework hybrid electrode over the routine electrodes is maintained as the current density is increased to up to 1.0 mA cm^{-2} (Figure 8D).[166]

Introducing transition metals, such as Co and Mn, to N-doped graphene can further intensify its lithiophilicity.[167,168] A CoN_x-doped carbon (CoNC) material contains Co single atoms each coordinated with 4 N dopant atoms in the graphene sheet (Figure 9A). The binding energy of such an atomic structure with Li atom can be stronger than N-doped graphene by 0.72 eV (Figure 9B), thanks to the formation of both Li–Co and Li–N bonds confirmed via differential charge density analysis.[167] Consequently, the Li deposition overpotential is significantly smaller for the CoNC electrode than a routine Cu electrode or a N-doped graphene matrix (NGM) electrode (Figure 9C).[167] This low nucleation overpotential, together with the guiding effect that regulates Li deposition location, results in uniformly distributed nucleation sites (Figure 9D), where subsequent Li^+ ions tend to adsorb and grow.[167] When these nucleation sites are close enough to each other, the separately deposited Li metal will eventually merge and give a smooth plating morphology, without the formation of Li dendrite. This is evidenced by scanning electron microscopy (SEM), which reveals that Li is plated evenly on the CoNC electrode (Figure 9E) but grows in the shape of filaments on the Cu electrode (Figure 9F).[167]

Beyond small DFT models involving binding energy calculations, lithiophilicity of doped graphene has also

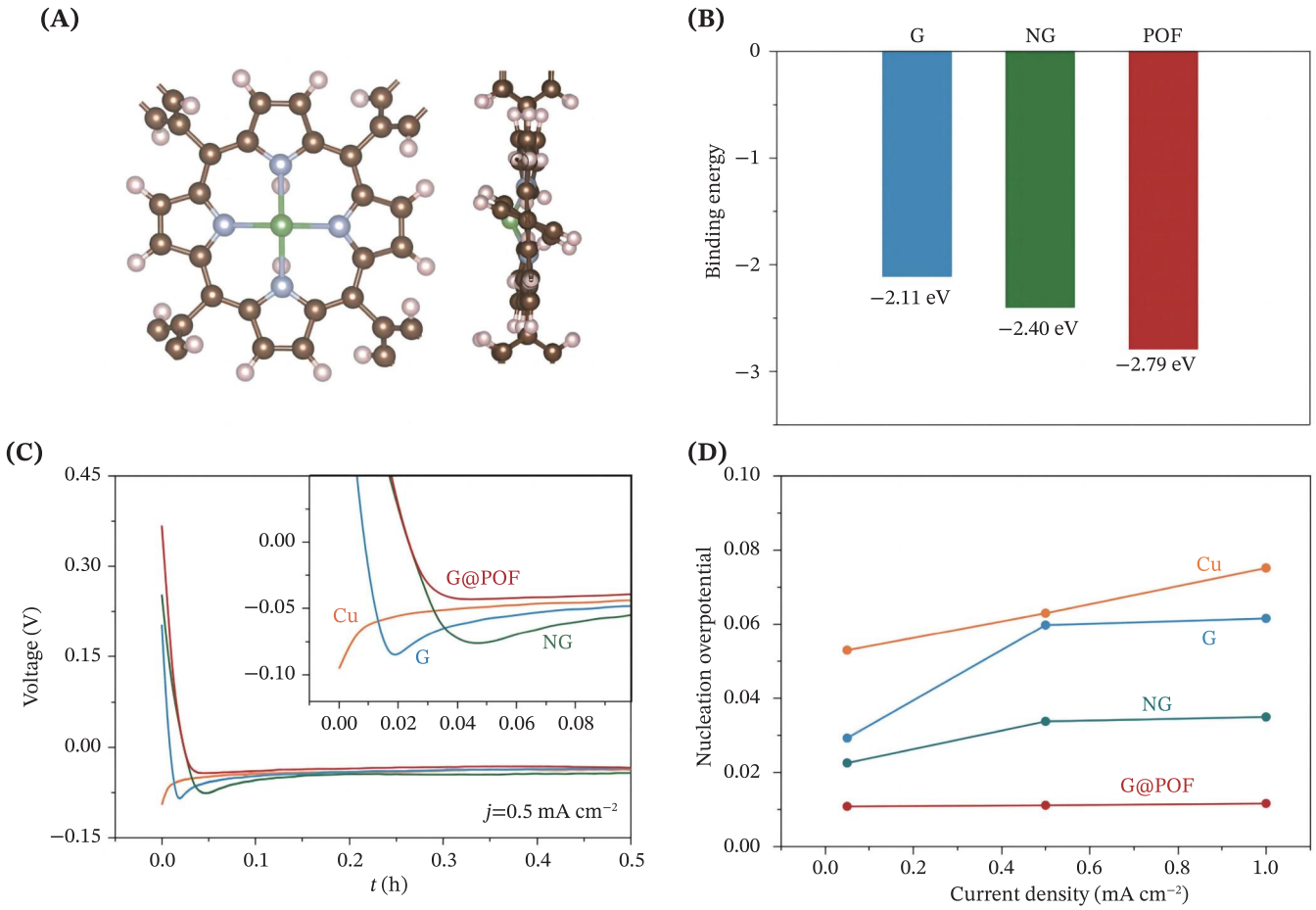

FIGURE 8 Favorable Li nucleation on a hybrid of graphene and porphyrin framework. (A) Optimized binding structure of Li and porphyrin viewed from top and side. Atom colors: brown, C; white, H; blue, N; green, Li. (B) Binding energy of graphene (G), N-doped graphene (NG), and porphyrin framework (POF) with Li. (C) Voltage plotted against time upon Li nucleation on electrodes made of Cu, G, NG, and porphyrin framework at graphene (G@POF) at a current density of 0.5 mA cm^{-2}. (D) Lithium nucleation overpotentials at various current densities for the four types of electrode materials. Reprinted with permission.[166] Copyright 2019, The Authors, published by the American Association for the Advancement of Science.

been elucidated on the scale of electric double layer (EDL) using MD simulations (Figure 10).[169] Given the small computational cost per atom and the flexibility of assigning charges to electrode atoms compared to DFT-based AIMD, classical MD is capable of modeling EDL evolution with electrode potential, including the distribution of ions and solvent molecules.[170] As a result, Li^+ is four times as likely to be found near a dopant N atom as to be found near a C atom in the EDL region between a N-doped graphene and a carbonate-based electrolyte solution.[169] This is further elucidated by the potential energy pit (0.04 eV stronger than C) and increased force of attraction (15% stronger than C) provided by the dopant N atoms to Li^+.[169] These results further suggest that N-doped graphene has the potential to guide Li^+ deposition by attracting Li^+ to the dopant sites even with the presence of solvent molecules and a working electrode potential.[169]

Apart from serving as the base for Li deposition as discussed above, it is also of interest to investigate the possibility of using graphene as a protective film placed on top of the Li metal anode. To serve as a protective film, the graphene layer must be capable of allowing Li^+ to penetrate while isolating the anode from the other electrolyte species. According to DFT calculations, the energy barrier for a Li^+ to penetrate a graphene layer through a hexagonal hole between 6 neighboring C atoms can be as high as 7.92 eV (Figure 11).[171] This is virtually impermeable to Li^+ or any other electrolyte species. However, this energy barrier can be lowered to 3.60, 2.98, or even 1.31 eV by introducing single vacancy (SV), Stone–Thrower–Wales (STW) defect, or double vacancy (DV), respectively, which provides a wider passage for Li^+ transport at the cost of mechanical strength.[171] When placed next to the Li metal anode, the protective layer can exhibit an even lower energy barrier due to the metal

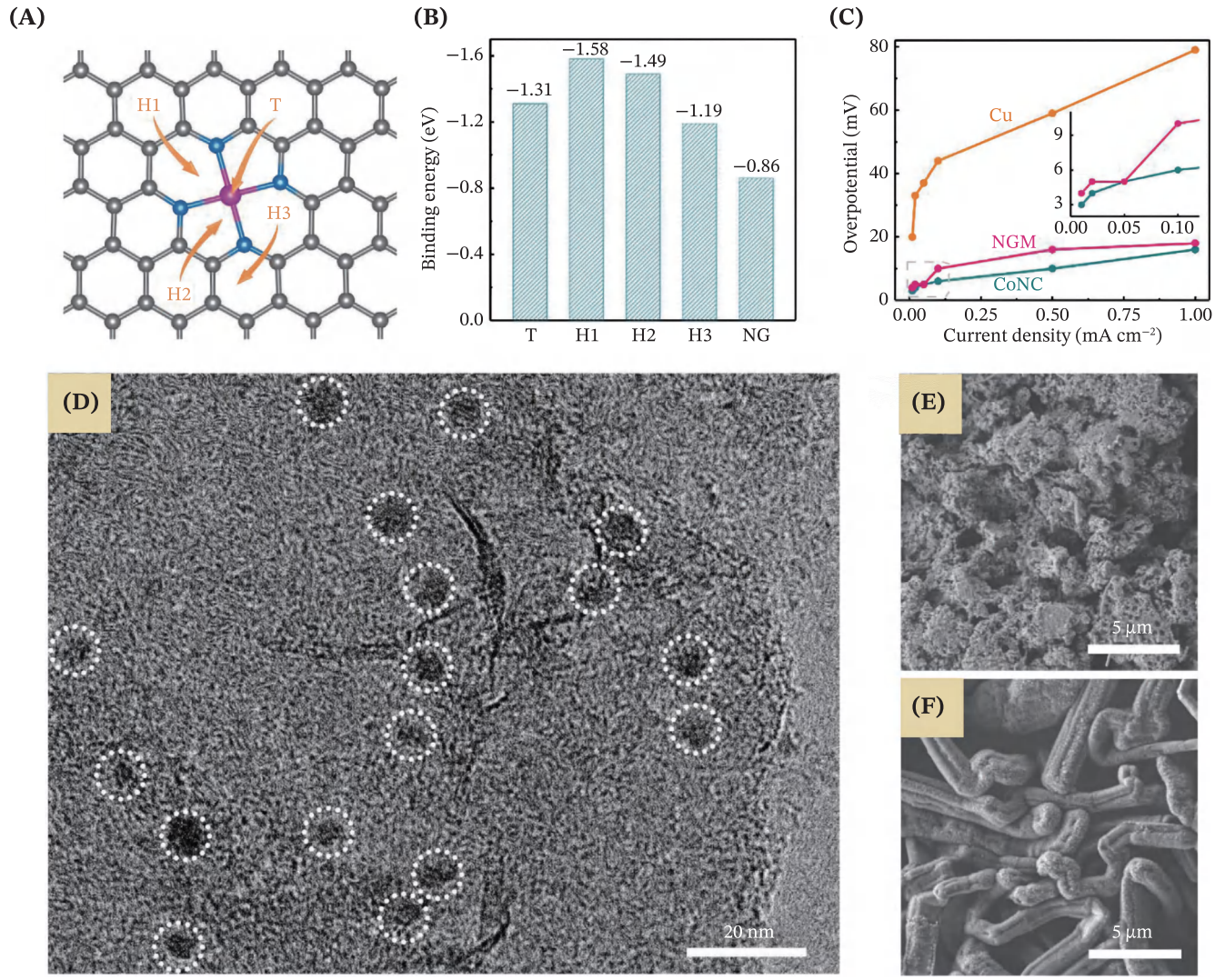

FIGURE 9 Li deposition morphology regulated by lithiophilic CoNC sites. (A) Li^+ adsorption sites at CoNC. Atom colors: gray, C; blue, N; purple, Co. (B) Binding energies of a Li atom at the four adsorption sites shown in (A) in comparison to its binding energy with N-doped graphene (NG). (C) Li nucleation overpotentials on Cu, NGM, and CoNC electrodes at various current densities. The inset is an enlarged picture of the region enclosed in the gray dashed box. (D) Transmission electron microscopy image of Li nucleation sites on CoNC after 5 min of charging at 0.1 mA cm^{-2}. SEM image of Li deposition morphology after 4 h of plating at 0.5 mA cm^{-2} on the (E) CoNC and (F) Cu electrodes. Reprinted with permission.[167] Copyright 2018, Wiley-VCH.

proximity effect.[171] For instance, the energy barrier for Li^+ to penetrate through SV is lowered from 3.60 eV to only 1.91 eV when coupled with Li (111) surface.[171]

4.4 | 3D carbon

Due to its abundance and ability of allowing reversible Li^+ intercalation, graphite is employed as the most common anode material in LIBs, with its fully lithiated form being LiC_6.[2] A DFT survey on crystal structures of Li carbides with different stoichiometries showed that LiC_4, LiC_5, LiC_6, LiC_8, LiC_{10}, and LiC_{12} are possible intercalation products at ambient pressure, with LiC_6 and LiC_{12} being thermodynamically stable.[172] The crystal structures of these two stable compounds are illustrated in Figure 12. LiC_4 or LiC_5 tends to decompose into LiC_6 and Li metal, while LiC_8 or LiC_{10} tends to decompose into LiC_6 and LiC_{12}.[172] This series of DFT calculations helps to explain why graphite can be intercalated stably up to LiC_6. As Li atoms are intercalated into graphite, more electrons are transferred to the sp^2 orbitals of C atoms, so the C–C bonds are elongated.[172] Bader charge analysis from AIMD snapshots indicates that Li atoms exist as $Li^{+0.6}$, $Li^{+0.7}$, and $Li^{+0.8}$ in LiC_{18}, LiC_{12}, and LiC_6, respectively.[173] At the same time, the distance between graphene layers increases from 3.35 Å (AB stacking) in pure graphite to ~3.7 Å (AA stacking) in intercalated

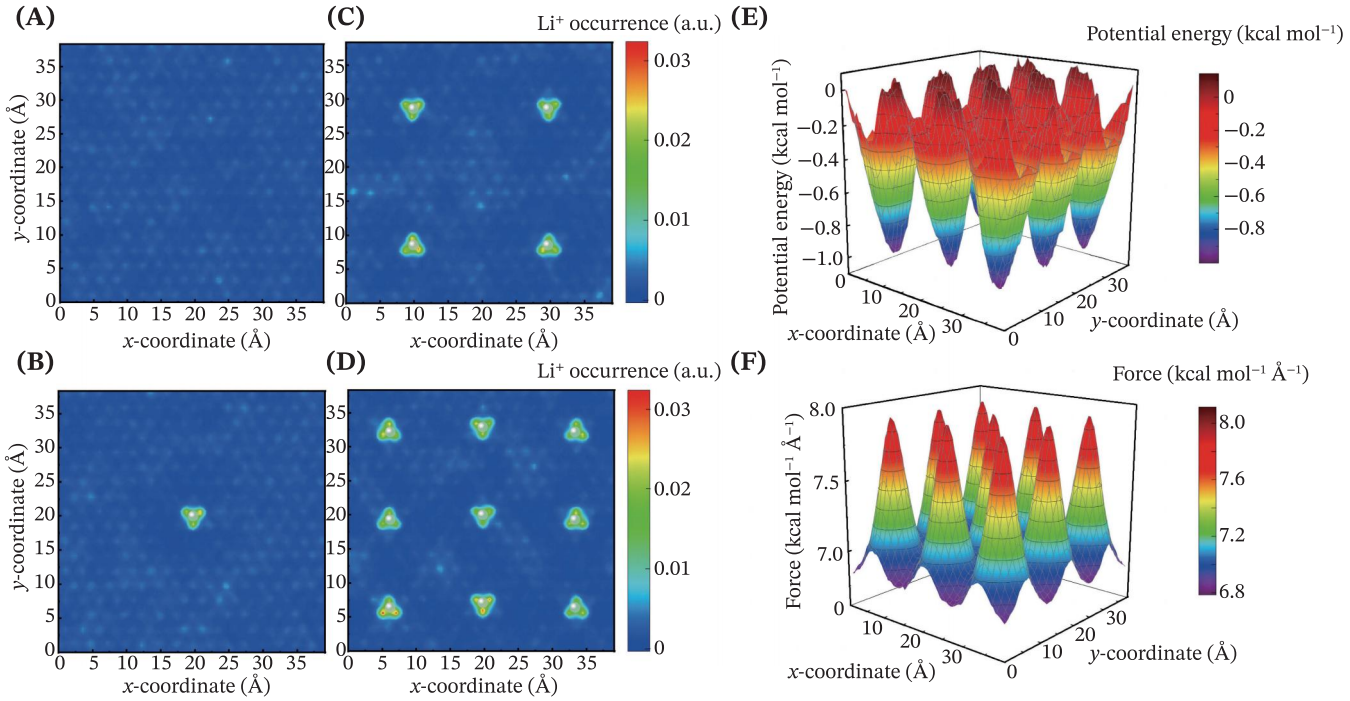

FIGURE 10 MD simulation of EDL structure reveals preferential Li^+ adsorption sites provided by dopant N atoms in graphene. The probability of finding Li^+ on the surface of graphene doped with (A) no N atom, (B) 1 N atom, (C) 4 N atoms, and (D) 9 N atoms among a total number of 576 atoms. Dopant N atoms are denoted by gray spheres. Potential energy (E) and force (F) landscape of a Li^+ near a graphene sheet doped with 9 N atoms. Reprinted with permission.[169] Copyright 2024, Science Press and Dalian Institute of Chemical Physics, Chinese Academy of Sciences.

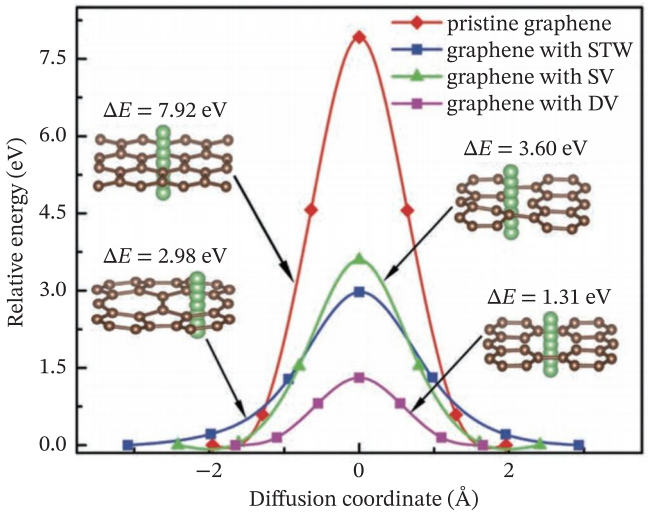

FIGURE 11 Potential energy evolution when a Li^+ diffuses in the direction perpendicular to the sheet of pristine or defective graphene. Three types of defects are investigated: STW defect, SV, and DV. Reprinted with permission.[171] Copyright 2017, Wiley-VCH.

compounds.[173] Since first-principles modeling of the Li–C system can be computationally expensive, machine learning potentials[174,175] have also been proposed for the intercalation structures at various conditions, aiming at reducing the computational cost while preserving electronic accuracy.[176] A neural-network potential has also been developed for carbon materials with various types of vacancy defects.[177]

The performance of graphite anode in LIBs depends greatly on its interaction with the working electrolyte. On the one hand, the EDL formed between the graphite anode and the liquid electrolyte upon their initial contact determines the composition of the SEI formed subsequently.[178] As revealed by MD simulations of the anode–electrolyte interface, strongly polar solvent molecules such as EC are enriched at the charged anode surface, compared to the less polar solvent dimethyl carbonate (DMC), leading to the dominance of EC decomposition compounds in SEI layers.[179,180] AIMD simulations have also suggested the possibility of electrochemical decomposition of PF_6^-, accompanied by the widely accepted thermal decomposition and decomposition induced by trace water.[181]

On the other hand, the graphite anode–electrolyte interface has significant implications for the transport of Li^+ in the whole cell. Upon charging, Li^+ ions travel out of the cathodes into the electrolyte, while Li^+ in the electrolyte phase intercalate into the graphite layers. Li^+

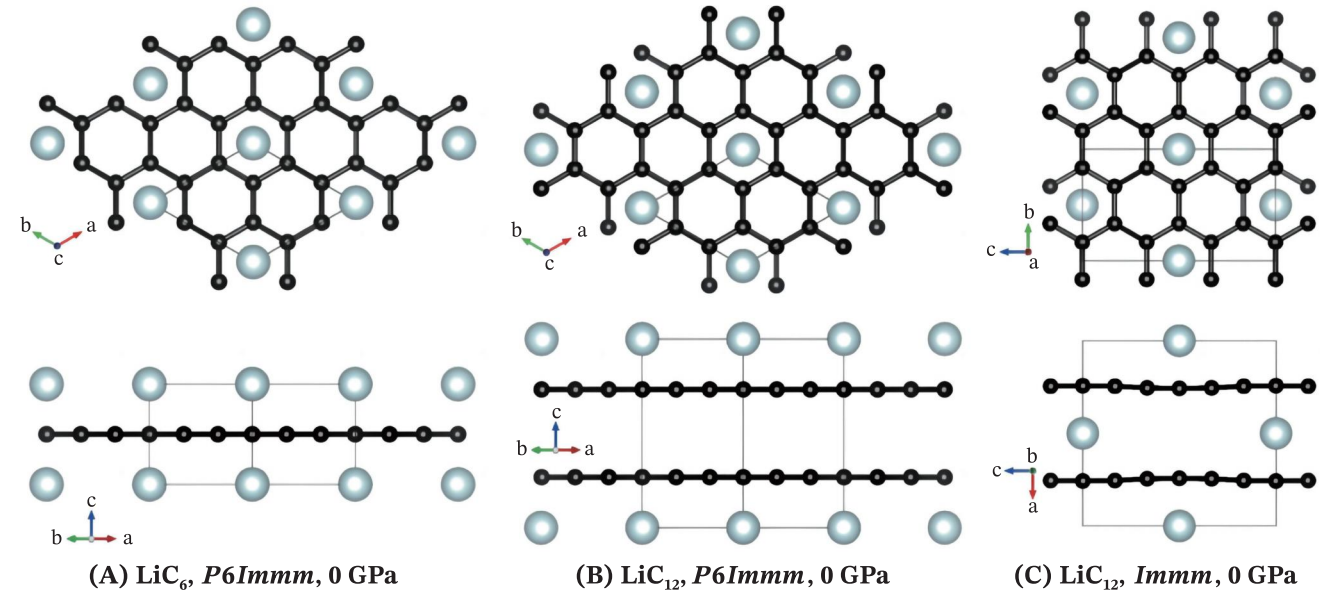

FIGURE 12 Crystal structures of stable Li-intercalated graphite. (A) Crystal structure of LiC_6. (B) Thermodynamically stable crystal structure of LiC_{12} with AAα stacking sequence, A denoting graphite and α denoting Li. (C) Metastable crystal structure of LiC_{12} with AαAβ stacking sequence, α and β denoting Li. Reprinted with permission.[172] Copyright 2015, American Physical Society.

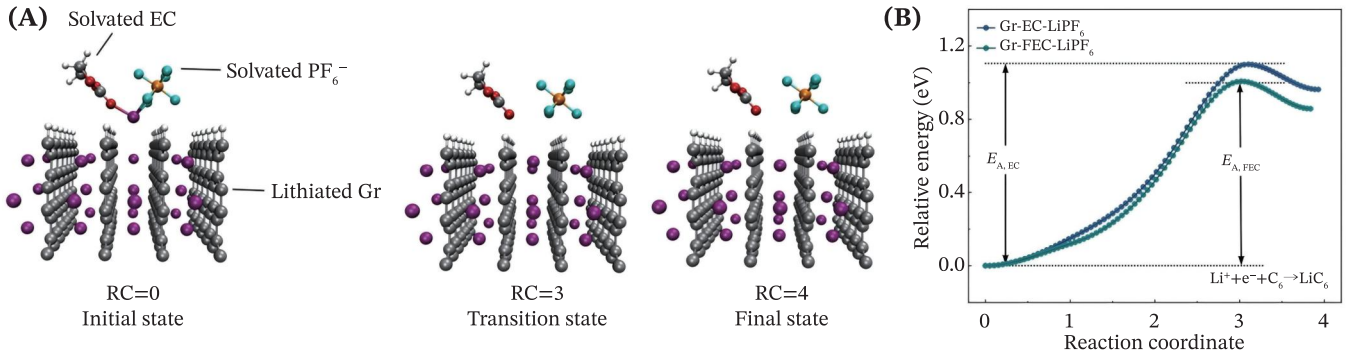

FIGURE 13 CI-NEB calculation scheme to determine the Li^+ intercalation energy barrier. (A) Atomic configurations at various reaction coordinates (RCs) during Li^+ desolvation and insertion between the graphite layers. (B) Relative energy versus RC when Li^+ is solvated by an EC or FEC molecule in addition to a PF_6^- anion. Reprinted with permission.[182] Copyright 2022, Wiley-VCH.

intercalation kinetics at the graphite electrode plays a vital role in dictating the rate performance and low-temperature compatibility of the LIB. To intercalate into graphite, Li^+ in the solution needs to escape from its solvation shell, passing from the outer Helmholtz plane into the inner Helmholtz plane. This is an energy-demanding event that requires an electric field at a relatively low electrode potential (e.g., ~1.4–3 V below the potential of zero charge), according to MD simulations of the EDL.[179,180] When coupled with a cathode with fast interfacial kinetics and a low energy barrier, such as the $LiNi_{0.8}Co_{0.15}Al_{0.05}O_2$ cathode interfacing with a LiTFSI–EC–DMC electrolyte solution, a high current density (e.g., 4.0 C) would result in Li plating on the graphite anode.[182,183] To mitigate this issue, weakly solvating fluoroethylene carbonate (FEC) can be employed instead of EC, which facilitates Li^+ intercalation into the graphite anode.[182] DFT calculations based on the climbing-image nudged elastic band (CI-NEB) method (Figure 13) reveal that FEC offers a lower energy barrier (1.01 eV) for Li^+ intercalation than EC (1.10 eV), thanks to the electron-withdrawing effect of the F atom from the coordinating carbonyl O atom.[182] PF_6^- was also included in the solvation shell in this calculation, because adding PF_6^- to the LiTFSI electrolyte increases the energy barrier of the cathode Li^+ transport, ultimately balancing the kinetics of the two electrodes.[182]

Another common issue upon Li intercalation is the exfoliation of graphite layers due to the co-insertion of Li^+ and solvent molecules. Since the attraction between

Li^+ and solvent molecules is very strong due to coordination, Li^+ can potentially drag solvent molecules into the space between graphite layers. The attraction between Li^+ and solvent can be weakened by applying a high concentration of LiTFSI, using low-solubility solvent, or adding NO_3^-.[184] MD simulations reveal that NO_3^- can replace $TFSI^-$ and solvent molecules in the first solvation shell.[184] Including NO_3^- in the solvation shell also makes the solvation cluster negatively charged, leading to the formation of large aggregates.[184] Consequently, the interaction between Li^+ and solvent molecules is effectively lowered, and graphite stability is practically enhanced.[184]

In LMBs, 3D carbon hosts have been implemented to move beyond the capacity limit of LIBs while mitigating dendrite and volume change problems of anodes consisting purely of Li metal. For instance, carbon fibers can be combined with Li metal to make a composite anode, in which a thin layer of LiC_6 is formed in situ on the surface of the carbon fibers.[30] While the carbon fiber is lithiophobic in nature, this LiC_6 layer is lithiophilic with a low nucleation overpotential of only 10 mV.[30]

Porous carbon, another anode host material, can be doped with N atoms by activating C_{60} molecules with KOH in an ammonia atmosphere.[185] Such treatment opens up the sphere structure of C_{60}, resulting in a large number of curved surfaces with defects doped with N atoms.[185] To illustrate the interaction between this material and Li^+, adsorption energy was calculated using DFT. On the one hand, the curved structure of C atoms was shown to adsorb Li^+ more strongly (−2.51 eV) than a flat graphene fragment (−1.88 eV).[185] On the other hand, N-doping, especially pyrrolic N, can significantly contribute to Li^+ storage capacity by strengthening the adsorption energy from −2.31 eV for pristine C_{60} to −5.56 eV.[185] Additionally, a nonlocal density functional theory (NLDFT) model was employed to determine the pore volume and pore size distribution, which agreed with X-ray diffraction (XRD) results.[185] Thanks to the pores and lithiophilicity, this anode achieves an improved capacity of ca. 1900 mA h g^{-1} at a current of 100 mA g^{-1},[185] which is much higher than the capacities of routine graphene (770–1115 mA h g^{-1}), CNTs (1115 mA h g^{-1}), or hard carbon (200–600 mA h g^{-1}) anodes.[186]

A more complex 3D carbon host structure has also been engineered by stacking layers of porous reduced graphene oxide, each layer further modified with N-doped nanoarrays.[131] The N dopant atoms lower the Li nucleation overpotential, while the well-aligned nanoarrays regulate the Li^+ flux by providing an optimized ion diffusion pathway.[131] The 3D structure with abundant nanoarrays also affords a large surface area to achieve a low current density, which further contributes to uniform Li plating.[131]

Table 1 summarizes the applications of the carbon materials discussed in this contribution, along with each material's advantages and disadvantages. The rational combination of carbon with active energy storage materials is strongly considered for efficient and effective Li storage in working batteries.

5 | CONCLUSIONS AND PERSPECTIVES

Using carbon materials as electrode materials in working batteries is one of the greenest and most effective ways for effective energy storage. The diversity of carbon materials is conducive to the efficient manifestation of energy–chemical processes at a macroscopic scale. Although they may not necessarily be the most central material in working devices, their superb electrical conductivity and diverse morphologies represent the limit of human control over materials, demonstrating our current controllability and precision under the scope of materials science.

The rich structures of carbon materials and doping strategies are bringing about abundant possibilities for emerging energy storage. Moreover, carbon materials are easy to be calculated theoretically in a high-throughput setting on computers. Consequently, artificial intelligence can be easily applied to empower the development of carbon-based energy materials.

In real devices, the role of carbon-based energy materials is multi-faceted. There is still room for applying in-situ characterization to understand the working behavior of energy materials at multiple scales and using advanced computation techniques to probe and clarify the potential of carbon-based energy materials.

The emerging energy devices have various application scenarios, requiring LIBs to play a role similar to that of chips in the sense that there is no one-size-fits-all design. Various kinds of energy materials designs are strongly requested for efficient energy storage in different scenarios. To accelerate knowledge discovery with big models, it is necessary to further explore the theoretical system for carbon-based energy materials, improve theoretical methods to conserve computational power, and introduce artificial intelligence into the computational systems and models.

Li battery technology has been empowered by carbon materials with various dimensionalities, namely 0D fullerenes and carbon capsules, 1D CNTs and GNRs, 2D graphene, 3D graphite and amorphous carbon, and the

TABLE 1 Typical applications of carbon materials in lithium batteries.

Carbon material	Application	Advantage	Disadvantage
0D fullerenes	Active material	Precise structure	High cost
			Low capacity
	Li storage	High capacity	High cost
	Protective film	Effective protection	High cost
	Additive precursor	Effective protection	High cost
Carbon capsules	Containment	Shuttle suppression	High cost
		Good conductivity	
		Volume buffer	
GNR derivatives	Conductive host	Good conductivity	High cost
	Adsorbent	Shuttle suppression	High cost
	Li storage	High capacity	High cost
		Volume buffer	
CNT derivatives	Conductive filler	Good conductivity	High cost
	Adsorbent	Shuttle suppression	High cost
	Li conductor	Dendrite suppression	High cost
	Current collector	Light weight	High cost
Graphene derivatives	Conductive host	Good conductivity	High cost
		Catalytic effects	
	Adsorbent	Shuttle suppression	High cost
	Li storage	High capacity	High cost
		Dendrite suppression	
	Protective film	Effective protection	Limited diffusion
Graphite	Li storage	Low cost	Limited capacity
		Good stability	
Porous carbon	Li storage	High capacity	High cost
	Na storage	Effective storage	Weak interaction
3D architectures	Conductive host	Good conductivity	High cost
		Shuttle suppression	
	Li storage	Volume buffer	High cost
		Dendrite suppression	

derivatives of the aforementioned materials. Employed in the battery's anode, cathode, electrolyte, and separator, their functions include but are not limited to conducting electrons and ions, storing Li, catalyzing electrochemical reactions, and protecting electrodes from undesired reactions. To probe their working mechanism and predict suitable design strategies, such as doping, defects, and structural design, theoretical models are extensively applied to reveal atomistic scenarios in bulk materials and interfaces. Specifically, DFT models are capable of predicting the carbon materials' conductivity, lithiophilicity, mechanical strength, transport energy barrier, charge transfer, and reaction pathway. MD simulations are capable of revealing the spatial distribution of molecules and coordination structures in bulk and interfaces, as well as their evolution with respect to changes in electrode potentials.

Noteworthily, there are still significant challenges in accurately modeling carbon materials in Li batteries due to limitations in computational power, especially when the scenario becomes more dynamic and less crystalline. Here are some important directions to explore:

1. *Accurate modeling of electrochemically active interfaces*. For instance, it is of great interest to predict SEI properties by modeling interfacial reactions, but this is quite challenging to accomplish with quantum accuracy. Machine learning interatomic potentials, such as

neural-network potentials, will be a powerful option to balance quantum accuracy and simulation timescale.
2. *Extending the research paradigm to battery systems beyond Li storage*. Atomistic scenarios are relatively underexplored when the carbon structure contains a significant degree of amorphism or other elements (such as MXenes), but such structures can be crucial for unlocking higher capacities and can be extended to Na- and K-storing systems.[187–190]
3. *Employing artificial intelligence to accelerate the discovery of novel carbon materials*. Thanks to the structural diversity of carbon materials and their potential to be engineered into advanced functional materials with nuanced designs, Li battery technology can expect significant inspiration from new breakthroughs in carbon material synthesis and characterization. During this process, knowledge discovery through machine learning based on high-throughput calculations and experiments will greatly assist in predicting working carbon materials for Li batteries, as it has already happened in some other fields including contaminant removal,[191] hydrogen energy,[192] and supercapacitors.[193]
4. *Modeling composite materials beyond mere carbon*. While carbon materials afford promising functions in lithium batteries, they are not the only class of materials that serves the purpose. Compositing carbon materials with other auxiliary materials, such as TiO_2,[194,195] can give full play to the potential of both materials. Theoretical investigations on the interplay between components remain underexplored.

Ultimately, clean energy is essential to sustainable development, and sustainable materials are strongly requested in clean energy systems. It is imperative to consider how to improve sustainability of materials from the perspectives of resources, energy, material recycling, dynamic reconfigurability, digital twins, and so forth. This also indicates unifying the matter–energy–information trinity to promote high-quality development of new energy through continuous theoretical innovation and original research paradigms.

AUTHOR CONTRIBUTIONS

Legeng Yu: Conceptualization, methodology, visualization, software, formal analysis, investigation, writing—original draft. **Xiang Chen**: Writing—review & editing, formal analysis, investigation, funding acquisition. **Nan Yao**: Conceptualization, formal analysis, investigation, writing—review & editing. **Yu-Chen Gao**: Methodology, investigation, writing—review & editing. **Yu-Hang Yuan**: Methodology, investigation, writing—review & editing. **Yan-Bin Gao**: Methodology, investigation, writing—review & editing. **Cheng Tang**: Writing—review & editing, investigation, funding acquisition. **Qiang Zhang**: Conceptualization, visualization, formal analysis, investigation, writing—review & editing, funding acquisition, supervision.

ACKNOWLEDGMENTS

This work was supported by Beijing Natural Science Foundation (L233004), the National Key Research and Development Program (2021YFB2500300), the National Natural Science Foundation of China (T2322015, 22109086, 52394170, 52394171, 22109011, 22393900, and 22108151), Tsinghua-Jiangyin Innovation Special Fund (TJISF) (2022JYTH0101), and the Tsinghua University Initiative Scientific Research Program.

CONFLICT OF INTEREST STATEMENT

The authors declare no conflict of interest.

ORCID

Qiang Zhang https://orcid.org/0000-0002-3929-1541

REFERENCES

1. Grey CP, Hall DS. Prospects for lithium-ion batteries and beyond—a 2030 vision. *Nat Commun*. 2020;11(1):6279.
2. Xie J, Lu Y-C. A retrospective on lithium-ion batteries. *Nat Commun*. 2020;11(1):2499.
3. Larcher D, Tarascon J-M. Towards greener and more sustainable batteries for electrical energy storage. *Nat Chem*. 2015;7(1):19-29.
4. Wulandari T, Fawcett D, Majumder SB, Poinern GEJ. Lithium-based batteries, history, current status, challenges, and future perspectives. *Battery Energy*. 2023;2(6):20230030.
5. Xin S, Zhang X, Wang L, et al. Roadmap for rechargeable batteries: present and beyond. *Sci China Chem*. 2024;67(1):13-42.
6. Cheng X-B, Liu H, Yuan H, et al. A perspective on sustainable energy materials for lithium batteries. *SusMat*. 2021;1(1):38-50.
7. Zhang S, Li S, Lu Y. Designing safer lithium-based batteries with nonflammable electrolytes: a review. *eScience*. 2021;1(2):163-177.
8. Kumar Prajapati A, Bhatnagar A. A review on anode materials for lithium/sodium-ion batteries. *J Energy Chem*. 2023;83:509-540.
9. Xu P, Shuang Z-Y, Zhao C-Z, et al. A review of solid-state lithium metal batteries through in-situ solidification. *Sci China Chem*. 2024;67(1):67-86.
10. Shen X, Zhang X-Q, Ding F, et al. Advanced electrode materials in lithium batteries: retrospect and prospect. *Energy Mater Adv*. 2021;2021:1205324.
11. Zhang X-Q, Zhao C-Z, Huang J-Q, Zhang Q. Recent advances in energy chemical engineering of next-generation lithium batteries. *Engineering*. 2018;4(6):831-847.
12. Jin C-B, Shi P, Zhang X-Q, Huang J-Q. Advances in carbon materials for stable lithium metal batteries. *New Carbon Mater*. 2022;37(1):1-24.

13. Cai W, Yao Y-X, Zhu G-L, et al. A review on energy chemistry of fast-charging anodes. *Chem Soc Rev*. 2020;49(12):3806-3833.
14. Chen L, Wu H, Ai X, Cao Y, Chen Z. Toward wide-temperature electrolyte for lithium-ion batteries. *Battery Energy*. 2022;1(2):20210006.
15. Rodrigues M-TF, Babu G, Gullapalli H, et al. A materials perspective on Li-ion batteries at extreme temperatures. *Nat Energy*. 2017;2(8):17108.
16. Li Z, Yao N, Yu L, et al. Inhibiting gas generation to achieve ultralong-lifespan lithium-ion batteries at low temperatures. *Matter*. 2023;6(7):2274-2292.
17. Lin D, Liu Y, Cui Y. Reviving the lithium metal anode for high-energy batteries. *Nat Nanotechnol*. 2017;12(3):194-206.
18. Xu B, Li X, Yang C, et al. Interfacial chemistry enables stable cycling of all-solid-state Li metal batteries at high current densities. *J Am Chem Soc*. 2021;143(17):6542-6550.
19. Xu W, Wang J, Ding F, et al. Lithium metal anodes for rechargeable batteries. *Energ Environ Sci*. 2014;7(2):513-537.
20. Mo R, Tan X, Li F, et al. Tin–graphene tubes as anodes for lithium-ion batteries with high volumetric and gravimetric energy densities. *Nat Commun*. 2020;11(1):1374.
21. Liu H, Cheng X, Yan C, et al. A perspective on energy chemistry of low-temperature lithium metal batteries. *iEnergy*. 2022;1(1):72-81.
22. Huang W-Z, Xu P, Huang X-Y, et al. Lithium metal anode: past, present, and future. *MetalMat*. 2024;1(1):e6.
23. Yang S-J, Jiang F-N, Hu J-K, et al. Life cycle safety issues of lithium metal batteries: a perspective. *Electron*. 2023;1(2):e8.
24. Huang J, Li F, Wu M, et al. Electrolyte chemistry for lithium metal batteries. *Sci China Chem*. 2022;65(5):840-857.
25. Yuan S, Kong T, Zhang Y, et al. Advanced electrolyte design for high-energy-density Li-metal batteries under practical conditions. *Angew Chem Int Ed*. 2021;60(49):25624-25638.
26. He Z, Chen Y, Huang F, et al. Fluorinated solvents for lithium metal batteries. *Acta Phys Chim Sin*. 2022;38:2205005.
27. Yang Y, Yan C, Huang J. Research progress of solid electrolyte interphase in lithium batteries. *Acta Phys Chim Sin*. 2021;37:2010076.
28. Zhang L, Zhu C, Yu S, Ge D, Zhou H. Status and challenges facing representative anode materials for rechargeable lithium batteries. *J Energy Chem*. 2022;66:260-294.
29. Rosolen JM, Decker F. Stress in carbon film electrodes during Li^+ electrochemical intercalation. *J Electrochem Soc*. 1996;143(8):2417-2421.
30. Shi P, Li T, Zhang R, et al. Lithiophilic LiC_6 layers on carbon hosts enabling stable Li metal anode in working batteries. *Adv Mater*. 2019;31(8):1807131.
31. Lee J, Lee TH, Jang HW, Park HS. Chemical modification of ordered/disordered carbon nanostructures for metal hosts and electrocatalysts of lithium-air batteries. *InfoMat*. 2022;4(1):e12268.
32. Li Z, Huang Y, Yuan L, Hao Z, Huang Y. Status and prospects in sulfur–carbon composites as cathode materials for rechargeable lithium–sulfur batteries. *Carbon*. 2015;92:41-63.
33. Han J-G, Hwang C, Kim SH, et al. An antiaging electrolyte additive for high-energy-density lithium-ion batteries. *Adv Energy Mater*. 2020;10(20):2000563.
34. Yan K, Lee H-W, Gao T, et al. Ultrathin two-dimensional atomic crystals as stable interfacial layer for improvement of lithium metal anode. *Nano Lett*. 2014;14(10):6016-6022.
35. Wu L, Yao X, Liu Y, et al. A g-C_3N_4-coated paper-based separator for sodium metal batteries. *J Solid State Electrochem*. 2021;25(4):1373-1381.
36. Yao N, Sun S-Y, Chen X, et al. The anionic chemistry in regulating the reductive stability of electrolytes for lithium metal batteries. *Angew Chem Int Ed*. 2022;61(52):e202210859.
37. Beltran SP, Cao X, Zhang J-G, Balbuena PB. Localized high concentration electrolytes for high voltage lithium-metal batteries: correlation between the electrolyte composition and its reductive/oxidative stability. *Chem Mater*. 2020;32(14):5973-5984.
38. Wang F, Sun Y, Cheng J. Switching of redox levels leads to high reductive stability in water-in-salt electrolytes. *J Am Chem Soc*. 2023;145(7):4056-4064.
39. Gao Y-C, Yao N, Chen X, et al. Data-driven insight into the reductive stability of ion–solvent complexes in lithium battery electrolytes. *J Am Chem Soc*. 2023;145(43):23764-23770.
40. Chen X, Bai Y-K, Zhao C-Z, Shen X, Zhang Q. Lithium bonds in lithium batteries. *Angew Chem Int Ed*. 2020;59(28):11192-11195.
41. Hou T-Z, Xu W-T, Chen X, Peng H-J, Huang JQ, Zhang Q. Lithium bond chemistry in lithium–sulfur batteries. *Angew Chem Int Ed*. 2017;56(28):8178-8182.
42. Feng S, Fu Z-H, Chen X, et al. An electrocatalytic model of the sulfur reduction reaction in lithium–sulfur batteries. *Angew Chem Int Ed*. 2022;61(52):e202211448.
43. Yao N, Chen X, Fu Z-H, Zhang Q. Applying classical, ab initio, and machine-learning molecular dynamics simulations to the liquid electrolyte for rechargeable batteries. *Chem Rev*. 2022;122(12):10970-11021.
44. Sundararaman R, Vigil-Fowler D, Schwarz K. Improving the accuracy of atomistic simulations of the electrochemical interface. *Chem Rev*. 2022;122(12):10651-10674.
45. Yao N, Chen X, Shen X, et al. An atomic insight into the chemical origin and variation of the dielectric constant in liquid electrolytes. *Angew Chem Int Ed*. 2021;60(39):21473-21478.
46. Yao N, Yu L, Fu Z-H, et al. Probing the origin of viscosity of liquid electrolytes for lithium batteries. *Angew Chem Int Ed*. 2023;62(41):e202305331.
47. Sakong S, Huang J, Eikerling M, Groß A. The structure of the electric double layer: atomistic versus continuum approaches. *Curr Opin Electrochem*. 2022;33:100953.
48. Eyvazi N, Biagooi M, Nedaaee OS. Molecular dynamics investigation of charging process in polyelectrolyte-based supercapacitors. *Sci Rep*. 2022;12(1):1098.
49. Lee HG, Kim SY, Lee JS. Dynamic observation of dendrite growth on lithium metal anode during battery charging/discharging cycles. *npj Comput Mater*. 2022;8(1):103.
50. Chen X, Shen X, Li B, et al. Ion–solvent complexes promote gas evolution from electrolytes on a sodium metal anode. *Angew Chem Int Ed*. 2018;57(3):734-737.
51. Feng S, Fu Z-H, Chen X, Zhang Q. A review on theoretical models for lithium–sulfur battery cathodes. *InfoMat*. 2022;4:e12304.
52. Matsumura Y, Wang S, Mondori J. Interactions between disordered carbon and lithium in lithium ion rechargeable batteries. *Carbon*. 1995;33(10):1457-1462.
53. Miranda D, Costa CM, Lanceros-Mendez S. Lithium ion rechargeable batteries: state of the art and future needs of

microscopic theoretical models and simulations. *J Electroanal Chem*. 2015;739:97-110.

54. Miranda D, Gonçalves R, Wuttke S, Costa CM, Lanceros-Méndez S. Overview on theoretical simulations of lithium-ion batteries and their application to battery separators. *Adv Energy Mater*. 2023;13(13):2203874.
55. Wu Y, He J, Yang L, et al. Multiscale and multiphysics theoretical model and computational method for lithium-ion batteries. *Energy Storage Sci Technol*. 2023;12(7):2141-2154.
56. Chen A, Wang Z, Vidaurre KLL, et al. Knowledge-reused transfer learning for molecular and materials science. *J Energy Chem*. 2024;98:149-168.
57. Fu Z-H, Chen X, Zhang Q. Review on the lithium transport mechanism in solid-state battery materials. *WIREs Comput Mol Sci*. 2023;13(1):e1621.
58. Chen X, Zhang Q. Atomic insights into the fundamental interactions in lithium battery electrolytes. *Acc Chem Res*. 2020; 53(9):1992-2002.
59. Amaral MM, Real CG, Yukuhiro VY, et al. In situ and operando infrared spectroscopy of battery systems: progress and opportunities. *J Energy Chem*. 2023;81:472-491.
60. Alvira D, Antorán D, Manyà JJ. Plant-derived hard carbon as anode for sodium-ion batteries: a comprehensive review to guide interdisciplinary research. *Chem Eng J*. 2022;447: 137468.
61. Chen X, Liu C, Fang Y, et al. Understanding of the sodium storage mechanism in hard carbon anodes. *Carbon Energy*. 2022;4(6):1133-1150.
62. Bommel S, Kleppmann N, Weber C, et al. Unravelling the multilayer growth of the fullerene C_{60} in real time. *Nat Commun*. 2014;5(1):5388.
63. Diener MD, Alford JM. Isolation and properties of small-bandgap fullerenes. *Nature*. 1998;393(6686):668-671.
64. Haddon RC, Hebard AF, Rosseinsky MJ, et al. Conducting films of C_{60} and C_{70} by alkali-metal doping. *Nature*. 1991; 350(6316):320-322.
65. Hebard AF, Rosseinsky MJ, Haddon RC, et al. Superconductivity at 18 K in potassium-doped C_{60}. *Nature*. 1991;350(6319): 600-601.
66. Ramirez AP. Superconductivity in alkali-doped C_{60}. *Physica C Supercond*. 2015;514:166-172.
67. Schön JH, Kloc C, Siegrist T, Steigerwald M, Svensson C, Batlogg B. Superconductivity in single crystals of the fullerene C_{70}. *Nature*. 2001;413(6858):831-833.
68. Tanigaki K, Ebbesen TW, Saito S, et al. Superconductivity at 33 K in $Cs_xRb_yC_{60}$. *Nature*. 1991;352(6332):222-223.
69. Kim TJ, Yoon JH, Yi G-R, Yoo PJ. Si nanoparticle clusters in hollow carbon capsules (SNC@C) as lithium battery anodes: toward high initial coulombic efficiency. *Nanoscale*. 2019; 11(28):13650-13658.
70. Zhang S, Ao X, Huang J, et al. Isolated single-atom Ni–N_5 catalytic site in hollow porous carbon capsules for efficient lithium–sulfur batteries. *Nano Lett*. 2021;21(22):9691-9698.
71. Xiao Z, Yu Z, Ma X, Xu C. S,N-codoped carbon capsules with microsized entrance: highly stable S reservoir for Li–S batteries. *Adv Powder Technol*. 2021;32(5):1757-1765.
72. Chen Z, Narita A, Müllen K. Graphene nanoribbons: on-surface synthesis and integration into electronic devices. *Adv Mater*. 2020;32(45):2001893.
73. Wang H, Wang HS, Ma C, et al. Graphene nanoribbons for quantum electronics. *Nat Rev Phys*. 2021;3(12):791-802.
74. Gu Y, Qiu Z, Müllen K. Nanographenes and graphene nanoribbons as multitalents of present and future materials science. *J Am Chem Soc*. 2022;144(26):11499-11524.
75. Saraswat V, Jacobberger RM, Arnold MS. Materials science challenges to graphene nanoribbon electronics. *ACS Nano*. 2021;15(3):3674-3708.
76. Huang LF, Zhang GR, Zheng XH, et al. Understanding and tuning the quantum-confinement effect and edge magnetism in zigzag graphene nanoribbon. *J Phys Condens Matter*. 2013; 25:055304.
77. Mota EAV, da Silva CAB, Del Nero J. Theoretical investigation of width effects in the electronic and transport properties of carbon nanoribbons with 5–8–5 carbon rings: a first-principles study. *J Mater Chem C*. 2024;12(4):1459-1473.
78. Bang K, Chee S-S, Kim K, et al. Effect of ribbon width on electrical transport properties of graphene nanoribbons. *Nano Converg*. 2018;5(1):7.
79. Yang L, Park C-H, Son Y-W, Cohen ML, Louie SG. Quasiparticle energies and band gaps in graphene nanoribbons. *Phys Rev Lett*. 2007;99(18):186801.
80. Kosynkin DV, Lu W, Sinitskii A, Pera G, Sun Z, Tour JM. Highly conductive graphene nanoribbons by longitudinal splitting of carbon nanotubes using potassium vapor. *ACS Nano*. 2011;5(2):968-974.
81. Son Y-W, Cohen ML, Louie SG. Half-metallic graphene nanoribbons. *Nature*. 2006;444(7117):347-349.
82. Aprojanz J, Power SR, Bampoulis P, et al. Ballistic tracks in graphene nanoribbons. *Nat Commun*. 2018;9(1):4426.
83. Baringhaus J, Ruan M, Edler F, et al. Exceptional ballistic transport in epitaxial graphene nanoribbons. *Nature*. 2014; 506(7488):349-354.
84. Qin L-C. Determination of the chiral indices (*n,m*) of carbon nanotubes by electron diffraction. *Phys Chem Chem Phys*. 2007;9(1):31-48.
85. Slepyan GY, Maksimenko SA, Lakhtakia A, Yevtushenko O, Gusakov AV. Electrodynamics of carbon nanotubes: dynamic conductivity, impedance boundary conditions, and surface wave propagation. *Phys Rev B*. 1999;60(24):17136-17149.
86. Ebbesen TW, Lezec HJ, Hiura H, Bennett JW, Ghaemi HF, Thio T. Electrical conductivity of individual carbon nanotubes. *Nature*. 1996;382(6586):54-56.
87. Javey A, Guo J, Wang Q, Lundstrom M, Dai H. Ballistic carbon nanotube field-effect transistors. *Nature*. 2003;424(6949): 654-657.
88. White CT, Todorov TN. Carbon nanotubes as long ballistic conductors. *Nature*. 1998;393(6682):240-242.
89. Zhao M-Q, Liu X-F, Zhang Q, et al. Graphene/single-walled carbon nanotube hybrids: one-step catalytic growth and applications for high-rate Li–S batteries. *ACS Nano*. 2012;6(12): 10759-10769.
90. He Z, Xiao Z, Yue H, et al. Single-walled carbon nanotube film as an efficient conductive network for Si-based anodes. *Adv Funct Mater*. 2023;33(26):2300094.
91. Dressler RA, Dahn JR. Optimization of Si-containing and SiO based anodes with single-walled carbon nanotubes for high energy density applications. *J Electrochem Soc*. 2024;171(3): 030520.

92. Lim SH, Li R, Ji W, Lin J. Effects of nitrogenation on single-walled carbon nanotubes within density functional theory. *Phys Rev B*. 2007;76(19):195406.
93. Castro Neto AH, Guinea F, Peres NMR, Novoselov KS, Geim AK. The electronic properties of graphene. *Rev Mod Phys*. 2009;81(1):109-162.
94. Rizzi L, Zienert A, Schuster J, Köhne M, Schulz SE. Electrical conductivity modeling of graphene-based conductor materials. *ACS Appl Mater Interfaces*. 2018;10(49):43088-43094.
95. Xu H, Ma L, Jin Z. Nitrogen-doped graphene: synthesis, characterizations and energy applications. *J Energy Chem*. 2018;27(1):146-160.
96. Yuan Y, Zhang L, Xing J, et al. High-yield synthesis and optical properties of g-C_3N_4. *Nanoscale*. 2015;7(29):12343-12350.
97. Wudil YS, Ahmad UF, Gondal MA, et al. Tuning of graphitic carbon nitride (g-C_3N_4) for photocatalysis: a critical review. *Arab J Chem*. 2023;16(3):104542.
98. Zhang Y, Mori T, Ye J, Antonietti M. Phosphorus-doped carbon nitride solid: enhanced electrical conductivity and photocurrent generation. *J Am Chem Soc*. 2010;132(18):6294-6295.
99. Dong G, Zhao K, Zhang L. Carbon self-doping induced high electronic conductivity and photoreactivity of g-C_3N_4. *Chem Commun*. 2012;48(49):6178-6180.
100. Lan Z-A, Zhang G, Wang X. A facile synthesis of br-modified g-C_3N_4 semiconductors for photoredox water splitting. *Appl Catal Environ*. 2016;192:116-125.
101. Zhang S, Li J, Zeng M, Li J, Xu J, Wang X. Bandgap engineering and mechanism study of nonmetal and metal ion codoped carbon nitride: C + Fe as an example. *Chem A Eur J*. 2014;20(31):9805-9812.
102. Sugihara K, Sato H. Electrical conductivity of graphite. *J Physical Soc Japan*. 1963;18(3):332-341.
103. Buerschaper RA. Thermal and electrical conductivity of graphite and carbon at low temperatures. *J Appl Phys*. 1944;15(5):452-454.
104. Pietronero L, Strassler S, Zeller HR. Electrical conductivity of a graphite layer. *Phys Rev B*. 1980;22(2):904-910.
105. Cermak M, Perez N, Collins M, Bahrami M. Material properties and structure of natural graphite sheet. *Sci Rep*. 2020;10(1):18672.
106. Dasgupta D, Demichelis F, Tagliaferro A. Electrical conductivity of amorphous carbon and amorphous hydrogenated carbon. *Philos Mag B*. 1991;63(6):1255-1266.
107. Qiu H, Wan J, Zhang J, et al. Probing mechanistic insights into highly efficient lithium storage of C_{60} fullerene enabled via three-electron-redox chemistry. *Adv Sci*. 2021;8:2101759.
108. Seger L, Wen LQ, Schlenoff JB. Prospects for using C_{60} and C_{70} in lithium batteries. *J Electrochem Soc*. 1991;138(12):L81-L82.
109. Hudaya C, Halim M, Pröll J, et al. A polymerized C_{60} coating enhancing interfacial stability at three-dimensional $LiCoO_2$ in high-potential regime. *J Power Sources*. 2015;298:1-7.
110. Peng H-J, Huang J-Q, Cheng X-B, Zhang Q. Review on high-loading and high-energy lithium–sulfur batteries. *Adv Energy Mater*. 2017;7(24):1700260.
111. An Y, Tian Y, Fei H, et al. Facile preparation of fullerene nanorods for high-performance lithium–sulfur batteries. *Mater Lett*. 2018;228:175-178.
112. Xia M, Zhang N, Ge C. Mesoporous hollow carbon capsules as sulfur hosts for highly stable lithium–sulfur batteries. *J Mater Sci*. 2020;55(22):9516-9524.
113. Yang Y, Li L, Fei H, Peng Z, Ruan G, Tour JM. Graphene nanoribbon/V_2O_5 cathodes in lithium-ion batteries. *ACS Appl Mater Interfaces*. 2014;6(12):9590-9594.
114. Hou T-Z, Peng H-J, Huang J-Q, Zhang Q, Li B. The formation of strong-couple interactions between nitrogen-doped graphene and sulfur/lithium (poly)sulfides in lithium–sulfur batteries. *2D Mater*. 2015;2(1):014011.
115. Hou T-Z, Chen X, Peng H-J, et al. Design principles for heteroatom-doped nanocarbon to achieve strong anchoring of polysulfides for lithium–sulfur batteries. *Small*. 2016;12(24):3283-3291.
116. Peng H-J, Hou T-Z, Zhang Q, et al. Strongly coupled interfaces between a heterogeneous carbon host and a sulfur-containing guest for highly stable lithium–sulfur batteries: mechanistic insight into capacity degradation. *Adv Mater Interfaces*. 2014;1(7):1400227.
117. Wu M-r, Gao M-y, Zhang S-y, et al. High-performance lithium–sulfur battery based on porous N-rich g-C_3N_4 nanotubes via a self-template method. *Int J Min Met Mater*. 2021;28(10):1656-1665.
118. Li Z, Yu L, Bi C-X, et al. A three-way electrolyte with ternary solvents for high-energy-density and long-cycling lithium–sulfur pouch cells. *SusMat*. 2024;4(2):e191.
119. Zhang Q, Huang J-Q, Qian W-Z, Zhang Y-Y, Wei F. The road for nanomaterials industry: a review of carbon nanotube production, post-treatment, and bulk applications for composites and energy storage. *Small*. 2013;9(8):1237-1265.
120. Yuan Z, Peng H-J, Huang J-Q, et al. Hierarchical free-standing carbon-nanotube paper electrodes with ultrahigh sulfur-loading for lithium–sulfur batteries. *Adv Funct Mater*. 2014;24(39):6105-6112.
121. Longo RC, Camacho-Forero LE, Balbuena PB. Li_2S growth on graphene: impact on the electrochemical performance of Li–S batteries. *J Chem Phys*. 2020;152(1):014701.
122. Su F, Yi Z, Xie L, et al. Critical role of surface defects in the controllable deposition of Li_2S on graphene: from molecule to crystallite. *ACS Appl Mater Interfaces*. 2020;12(47):53435-53445.
123. Li B-Q, Kong L, Zhao C-X, et al. Expediting redox kinetics of sulfur species by atomic-scale electrocatalysts in lithium–sulfur batteries. *InfoMat*. 2019;1(4):533-541.
124. Shi Y, Wen L, Pei S, Wu M, Li F. Choice for graphene as conductive additive for cathode of lithium-ion batteries. *J Energy Chem*. 2019;30:19-26.
125. Peng H-J, Huang J-Q, Zhao M-Q, et al. Nanoarchitectured graphene/CNT@porous carbon with extraordinary electrical conductivity and interconnected micro/mesopores for lithium-sulfur batteries. *Adv Funct Mater*. 2014;24(19):2772-2781.
126. Liang Y, Zhang W, Wu D, Ni Q-Q, Zhang MQ. Interface engineering of carbon-based nanocomposites for advanced electrochemical energy storage. *Adv Mater Interfaces*. 2018;5(14):1800430.
127. Kong L, Yan C, Huang J-Q. A review of nanocarbon current collectors used in electrochemical energy storage devices. *New Carbon Mater*. 2017;32(6):481-500.
128. Zhang X, Cheng X, Zhang Q. Nanostructured energy materials for electrochemical energy conversion and storage: a review. *J Energy Chem*. 2016;25(6):967-984.

129. Tang C, Wang H-F, Huang J-Q, et al. 3D hierarchical porous graphene-based energy materials: synthesis, functionalization, and application in energy storage and conversion. *Electrochem Energy Rev*. 2019;2(2):332-371.
130. Zou R, Liu W, Ran F. Sulfur-containing polymer cathode materials: from energy storage mechanism to energy density. *InfoMat*. 2022;4(8):e12319.
131. Lu R, Cheng M, Mao L, et al. Nitrogen-doped nanoarray-modified 3D hierarchical graphene as a cofunction host for high-performance flexible Li–S battery. *EcoMat*. 2020;2(1):e12010.
132. Liu X-Y, Peng H-J, Zhang Q, et al. Hierarchical carbon nanotube/carbon black scaffolds as short- and long-range electron pathways with superior Li-ion storage performance. *ACS Sustainable Chem Eng*. 2014;2(2):200-206.
133. Ni J, Zhang L, Fu S, Savilov SV, Aldoshin SM, Lu L. A review on integrating nano-carbons into polyanion phosphates and silicates for rechargeable lithium batteries. *Carbon*. 2015;92:15-25.
134. Shan C, Yen H-J, Wu K, et al. Functionalized fullerenes for highly efficient lithium ion storage: structure–property–performance correlation with energy implications. *Nano Energy*. 2017;40:327-335.
135. Teprovich JA Jr, Weeks JA, Ward PA, et al. Hydrogenated C_{60} as high-capacity stable anode materials for Li ion batteries. *ACS Appl Energy Mater*. 2019;2(9):6453-6460.
136. Xu Q, Lin J, Ye C, et al. Air-stable and dendrite-free lithium metal anodes enabled by a hybrid interphase of C_{60} and Mg. *Adv Energy Mater*. 2020;10(6):1903292.
137. Niu S, Zhang S-W, Li D, et al. Sandwiched Li plating between lithiophilic–lithiophobic gradient silver@fullerene interphase layer for ultrastable lithium metal anodes. *Chem Eng J*. 2022;429:132156.
138. Liu Z, Huang W, Xiao Y, et al. Nanocomposite current collectors for anode-free all-solid-state lithium batteries. *Acta Phys Chim Sin*. 2024;40:2305040.
139. Lee Y-G, Fujiki S, Jung C, et al. High-energy long-cycling all-solid-state lithium metal batteries enabled by silver–carbon composite anodes. *Nat Energy*. 2020;5(4):299-308.
140. Spencer-Jolly D, Agarwal V, Doerrer C, et al. Structural changes in the silver-carbon composite anode interlayer of solid-state batteries. *Joule*. 2023;7(3):503-514.
141. Song L, Li R, Zhu H, et al. Deeply lithiated carbonaceous materials for great lithium metal protection in all-solid-state batteries. *Adv Mater*. 2024;36(26):2400165.
142. Xie F, Diallo MS, Kim H, Tu QH, Ceder G. The microscopic mechanism of lithiation and delithiation in the Ag/C buffer layer for anode-free solid-state batteries. *Adv Energy Mater*. 2024;14(10):2302960.
143. Zhang R, Chen X, Shen X, et al. Coralloid carbon fiber-based composite lithium anode for robust lithium metal batteries. *Joule*. 2018;2(4):764-777.
144. Jiang Z, Zeng Z, Yang C, et al. Nitrofullerene, a C_{60}-based bifunctional additive with smoothing and protecting effects for stable lithium metal anode. *Nano Lett*. 2019;19(12):8780-8786.
145. Uthaisar C, Barone V, Peralta JE. Lithium adsorption on zigzag graphene nanoribbons. *J Appl Phys*. 2009;106(11):113715.
146. Liu Y, Wang X, Dong Y, Wang Z, Zhao Z, Qiu J. Nitrogen-doped graphene nanoribbons for high-performance lithium ion batteries. *J Mater Chem A*. 2014;2(40):16832-16835.
147. Li L, Kovalchuk A, Fei H, et al. Enhanced cycling stability of lithium-ion batteries using graphene-wrapped Fe_3O_4-graphene nanoribbons as anode materials. *Adv Energy Mater*. 2015;5(14):1500171.
148. Lin J, Peng Z, Xiang C, et al. Graphene nanoribbon and nanostructured SnO_2 composite anodes for lithium ion batteries. *ACS Nano*. 2013;7(7):6001-6006.
149. Fuchs T, Haslam CG, Moy AC, et al. Increasing the pressure-free stripping capacity of the lithium metal anode in solid-state-batteries by carbon nanotubes. *Adv Energy Mater*. 2022;12(26):2201125.
150. Liu Z, Liu Y, Miao Y, et al. Emerging carbon nanotube-based nanomaterials for stable and dendrite-free alkali metal anodes: challenges, strategies, and perspectives. *Energy Environ Mater*. 2023;6(6):e12525.
151. Fu Z-H, Chen X, Yao N, et al. Diameter-dependent ultrafast lithium-ion transport in carbon nanotubes. *J Chem Phys*. 2023;158(1):014702.
152. Garau C, Frontera A, Quiñonero D, Costa A, Ballester P, Deyà PM. Lithium diffusion in single-walled carbon nanotubes: a theoretical study. *Chem Phys Lett*. 2003;374(5-6):548-555.
153. Lv C, Tong Z, Zhou S-Y, et al. Spontaneous local redox reaction to passivate cnts as lightweight current collector for high energy density lithium ion batteries. *J Energy Chem*. 2023;80:553-561.
154. Chen S, Bao P, Xiao L, Wang G. Large-scale and low cost synthesis of graphene as high capacity anode materials for lithium-ion batteries. *Carbon*. 2013;64:158-169.
155. Pan D, Wang S, Zhao B, et al. Li storage properties of disordered graphene nanosheets. *Chem Mater*. 2009;21(14):3136-3142.
156. Huang C, Zhang S, Liu H, Li Y, Cui G, Li Y. Graphdiyne for high capacity and long-life lithium storage. *Nano Energy*. 2015;11:481-489.
157. Wang G, Shen X, Yao J, Park J. Graphene nanosheets for enhanced lithium storage in lithium ion batteries. *Carbon*. 2009;47(8):2049-2053.
158. Fan X, Zheng WT, Kuo J-L. Adsorption and diffusion of Li on pristine and defective graphene. *ACS Appl Mater Interfaces*. 2012;4(5):2432-2438.
159. Reddy ALM, Srivastava A, Gowda SR, Gullapalli H, Dubey M, Ajayan PM. Synthesis of nitrogen-doped graphene films for lithium battery application. *ACS Nano*. 2010;4(11):6337-6342.
160. Ma C, Shao X, Cao D. Nitrogen-doped graphene nanosheets as anode materials for lithium ion batteries: a first-principles study. *J Mater Chem*. 2012;22(18):8911-8915.
161. Zhang R, Cheng X-B, Zhao C-Z, et al. Conductive nanostructured scaffolds render low local current density to inhibit lithium dendrite growth. *Adv Mater*. 2016;28(11):2155-2162.
162. Zhang R, Chen X-R, Chen X, et al. Lithiophilic sites in doped graphene guide uniform lithium nucleation for dendrite-free lithium metal anodes. *Angew Chem Int Ed*. 2017;56(27):7764-7768.
163. Lv Q, Song R, Wang B, et al. Three-dimensional nitrogen-doped graphene aerogel toward dendrite-free lithium-metal anode. *Ionics*. 2020;26(1):13-22.

164. Chen X, Chen X-R, Hou T-Z, et al. Lithiophilicity chemistry of heteroatom-doped carbon to guide uniform lithium nucleation in lithium metal anodes. *Sci Adv*. 2019;5(2): eaau7728.
165. Chen X, Bai Y-K, Shen X, Peng H-J, Zhang Q. Sodiophilicity/-potassiophilicity chemistry in sodium/potassium metal anodes. *J Energy Chem*. 2020;51:1-6.
166. Li B-Q, Chen X-R, Chen X, et al. Favorable lithium nucleation on lithiophilic framework porphyrin for dendrite-free lithium metal anodes. *Research*. 2019;2019:4608940.
167. Liu H, Chen X, Cheng X-B, et al. Uniform lithium nucleation guided by atomically dispersed lithiophilic CoN_x sites for safe lithium metal batteries. *Small Methods*. 2019;3(9):1800354.
168. Liu X, Zhang Q, Ma Y, et al. MnO_2 nanosheet modified N, P co-doping carbon nanofibers on carbon cloth as lithiophilic host to construct high-performance anodes for Li metal batteries. *J Energy Chem*. 2022;69:270-281.
169. Yu L, Yao N, Gao Y-C, et al. Probing the electric double layer structure at nitrogen-doped graphite electrodes by constant-potential molecular dynamics simulations. *J Energy Chem*. 2024;93:299-305.
170. Yu L, Chen X, Yao N, Gao Y-C, Zhang Q. Constant-potential molecular dynamics simulation and its application in rechargeable batteries. *J Mater Chem A*. 2023;11(21):11078-11088.
171. Tian H, Seh ZW, Yan K, et al. Theoretical investigation of 2D layered materials as protective films for lithium and sodium metal anodes. *Adv Energy Mater*. 2017;7(13):1602528.
172. Lin Y, Strobel TA, Cohen RE. Structural diversity in lithium carbides. *Phys Rev B*. 2015;92(21):214106.
173. Jamnuch S, Pascal TA. Electronic signatures of lorentzian dynamics and charge fluctuations in lithiated graphite structures. *Nat Commun*. 2023;14(1):2291.
174. Mishin Y. Machine-learning interatomic potentials for materials science. *Acta Mater*. 2021;214:116980.
175. Deringer VL, Caro MA, Csányi G. Machine learning interatomic potentials as emerging tools for materials science. *Adv Mater*. 2019;31(46):1902765.
176. Babar M, Parks HL, Houchins G, Viswanathan V. An accurate machine learning calculator for the lithium-graphite system. *J Phys Energy*. 2021;3(1):014005.
177. Wang J, Shen H, Yang R, et al. A deep learning interatomic potential developed for atomistic simulation of carbon materials. *Carbon*. 2022;186:1-8.
178. Takenaka N, Suzuki Y, Sakai H, Nagaoka M. On electrolyte-dependent formation of solid electrolyte interphase film in lithium-ion batteries: strong sensitivity to small structural difference of electrolyte molecules. *J Phys Chem C*. 2014;118(20): 10874-10882.
179. Vatamanu J, Borodin O, Smith GD. Molecular dynamics simulation studies of the structure of a mixed carbonate/$LiPF_6$ electrolyte near graphite surface as a function of electrode potential. *J Phys Chem C*. 2012;116(1):1114-1121.
180. Boyer MJ, Vilciauskas L, Hwang GS. Structure and Li^+ ion transport in a mixed carbonate/$LiPF_6$ electrolyte near graphite electrode surfaces: a molecular dynamics study. *Phys Chem Chem Phys*. 2016;18(40):27868-27876.
181. Leung K. Predicting the voltage dependence of interfacial electrochemical processes at lithium-intercalated graphite edge planes. *Phys Chem Chem Phys*. 2015;17(3):1637-1643.
182. Yao Y-X, Chen X, Yao N, et al. Unlocking charge transfer limitations for extreme fast charging of Li-ion batteries. *Angew Chem Int Ed*. 2023;62(4):e202214828.
183. Liu Y, Shi H, Wu Z-S. Recent status, key strategies and challenging perspectives of fast-charging graphite anodes for lithium-ion batteries. *Energ Environ Sci*. 2023;16(11):4834-4871.
184. Ming J, Cao Z, Wahyudi W, et al. New insights on graphite anode stability in rechargeable batteries: Li ion coordination structures prevail over solid electrolyte interphases. *ACS Energy Lett*. 2018;3(2):335-340.
185. Tan Z, Ni K, Chen G, et al. Incorporating pyrrolic and pyridinic nitrogen into a porous carbon made from C_{60} molecules to obtain superior energy storage. *Adv Mater*. 2017;29(8):1603414.
186. Hossain MH, Islam MA, Chowdhury MA, Hossain N. Prospects and challenges of anode materials for lithium-ion batteries—a review. *Clean Energy Syst*. 2024;9:100145.
187. Yu T, Yang H, Cheng H-M, Li F. Theoretical progress of 2D six-membered-ring inorganic materials as anodes for non-lithium-ion batteries. *Small*. 2022;18(43):2107868.
188. Ding J, Li H, Wang S, et al. Vertical two-dimensional heterostructures and superlattices for lithium batteries and beyond. *Nano Energy*. 2024;129:110042.
189. Kumar S, Kumari N, Seo Y. Mxenes: versatile 2D materials with tailored surface chemistry and diverse applications. *J Energy Chem*. 2024;90:253-293.
190. Lei H, Li J, Zhang X, et al. A review of hard carbon anode: rational design and advanced characterization in potassium ion batteries. *InfoMat*. 2022;4(2):e12272.
191. Park S, Seok H, Oh D, et al. Machine learning-based prediction of adsorption capacity of metal-doped and undoped activated carbon: assessing the role of metal doping. *Chemosphere*. 2024;366:143495.
192. Ding R, Chen J, Chen Y, Liu J, Bando Y, Wang X. Unlocking the potential: machine learning applications in electrocatalyst design for electrochemical hydrogen energy transformation. *Chem Soc Rev*. 2024;53(23):11390-11461.
193. Wang T, Pan R, Martins ML, et al. Machine-learning-assisted material discovery of oxygen-rich highly porous carbon active materials for aqueous supercapacitors. *Nat Commun*. 2023;14(1):4607.
194. Ahmed ATA, Soni R, Ansari AS, et al. Biowaste-derived graphitic carbon interfaced TiO_2 as anode for lithium-ion battery. *Surf Interfaces*. 2022;35:102404.
195. Xia Y, Rong C, Yang X, Lu F, Kuang X. Encapsulating mo-doped TiO_2 anatase in N-doped amorphous carbon with excellent lithium storage performances. *Front Mater*. 2019;6:1.

AUTHOR BIOGRAPHIES

Legeng Yu received his Bachelor's and Master's degree from the University of Toronto in 2018 and 2021, respectively. He is now a PhD candidate in Prof. Qiang Zhang's group in the Department of Chemical Engineering, Tsinghua University. He is interested in battery electrochemistry and strives to understand the physical chemistry of battery interfaces with computational tools.

Xiang Chen gained his bachelor's and PhD degrees from the Department of Chemical Engineering at Tsinghua University in 2016 and 2021, respectively. He is currently an associate professor at Tsinghua University. His research interests focus on understanding the chemical mechanism and materials science in rechargeable batteries.

Qiang Zhang is a professor at Tsinghua University. His current research interests are advanced energy materials, including dendrite-free lithium metal anode, lithium sulfur batteries, and electrocatalysis, especially the structure design and full demonstration of advanced energy materials in working devices. He is the Editor-in-Chief of EES Batteries, Advisor Editor of *Angew Chem*, Associate Editor of *J Energy Chem*. He is sitting on the advisory board of *Joule*, *Chem Soc Rev*, *Matter*, *InfoMat*, *Adv Funct Mater*, *Adv Energy Mater*, *ChemSusChem*, *J Mater Chem A*, *Chem Commun*, *Energy & Fuels*, and so on.

How to cite this article: Yu L, Chen X, Yao N, et al. Advanced carbon as emerging energy materials in lithium batteries: A theoretical perspective. *InfoMat*. 2025;7(5):e12653. doi:10.1002/inf2.12653